Article

Developmental Cell

The DYT6 Dystonia Protein THAP1 Regulates Myelination within the Oligodendrocyte Lineage

Graphical Abstract

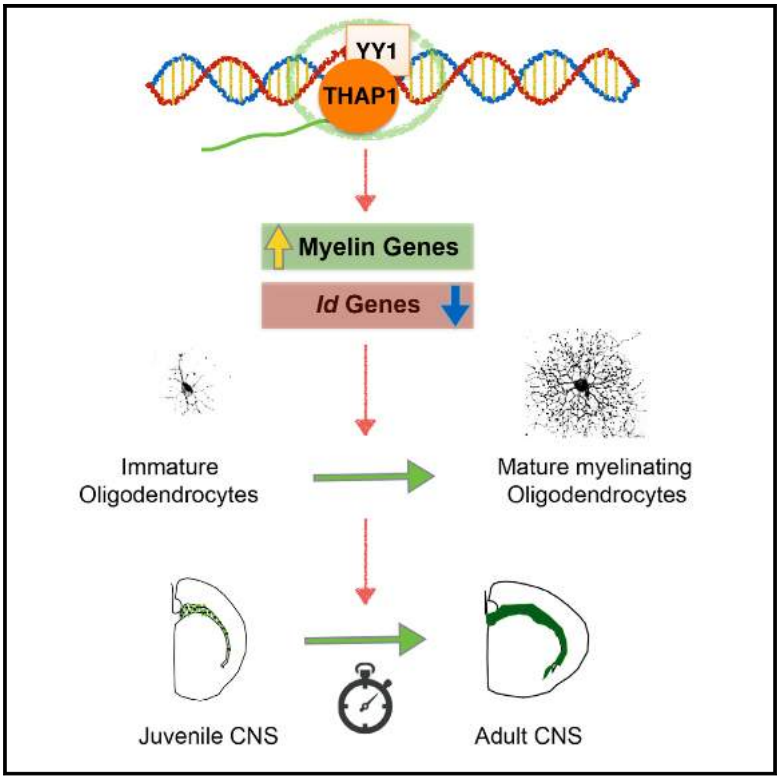

Authors

Dhananjay Yellajoshyula, Chun-Chi Liang, Samuel S. Pappas, ..., Stephanie Jou, Mark R. Cookson, William T. Dauer

Correspondence

dauer@med.umich.edu

In Brief

DYT6 dystonia is a motor disorder caused by loss-of-function mutations in the transcription factor THAP1. Yellajoshyula et al. demonstrate that loss of THAP1 impairs CNS myelination through a cell-autonomous role in the oligodendrocyte lineage and decreases the DNA occupancy of YY1, a transcription factor with an established role in myelination.

Highlights

- THAP1 is essential for the timing of myelination initiation during CNS maturation
- THAP1 affects myelination through a cell-autonomous role in oligodendrocytes
- THAP1 regulates DNA occupancy of the oligodendrocyte maturation factor YY1

Yellajoshyula et al., 2017, Developmental Cell *42*, 52–67
July 10, 2017
http://dx.doi.org/10.1016/j.devcel.2017.06.009

CellPress

Developmental Cell
Article

The DYT6 Dystonia Protein THAP1 Regulates Myelination within the Oligodendrocyte Lineage

Dhananjay Yellajoshyula,[1] Chun-Chi Liang,[1] Samuel S. Pappas,[1] Silvia Penati,[1] Angela Yang,[1] Rodan Mecano,[1] Ravindran Kumaran,[4] Stephanie Jou,[1] Mark R. Cookson,[4] and William T. Dauer[1,2,3,5,*]

[1]Department of Neurology, University of Michigan Medical School, 109 Zina Pitcher Place, Ann Arbor, MI 48109, USA
[2]Department of Cell and Developmental Biology, University of Michigan Medical School, 109 Zina Pitcher Place, Ann Arbor, MI 48109, USA
[3]VAAAHS, University of Michigan Medical School, University of Michigan, 109 Zina Pitcher Place, Ann Arbor, MI 48109, USA
[4]Cell Biology and Gene Expression Section, Laboratory of Neurogenetics, National Institute of Aging, National Institutes of Health, 9000 Rockville Pike, Bethesda, MD 20892, USA
[5]Lead Contact
*Correspondence: dauer@med.umich.edu
http://dx.doi.org/10.1016/j.devcel.2017.06.009

SUMMARY

The childhood-onset motor disorder DYT6 dystonia is caused by loss-of-function mutations in the transcription factor THAP1, but the neurodevelopmental processes in which THAP1 participates are unknown. We find that THAP1 is essential for the timing of myelination initiation during CNS maturation. Conditional deletion of THAP1 in the CNS retards maturation of the oligodendrocyte (OL) lineage, delaying myelination and causing persistent motor deficits. The CNS myelination defect results from a cell-autonomous requirement for THAP1 in the OL lineage and is recapitulated in developmental assays performed on OL progenitor cells purified from *Thap1* null mice. Loss of THAP1 function disrupts a core set of OL maturation genes and reduces the DNA occupancy of YY1, a transcription factor required for OL maturation. These studies establish a role for THAP1 transcriptional regulation at the inception of myelination and implicate abnormal timing of myelination in the pathogenesis of childhood-onset dystonia.

INTRODUCTION

Primary dystonia is characterized by isolated abnormal involuntary movements that typically cause prolonged twisting or turning of the involved body part (Tanabe et al., 2009). Many inherited forms of dystonia arise during childhood or young adulthood, indicating that the pathogenic mutations disrupt CNS maturation. Several causative genes have been identified, but the link between their disruption and abnormalities of specific neurodevelopmental events is poorly understood (Dauer, 2014). Absence of this knowledge limits understanding of motor circuit development and the ability to advance models of disease pathogenesis.

The prevailing view is that primary dystonia is caused by a "normal structure, abnormal function" pathogenic mechanism, based largely on normal appearing traditional neuroimaging and very few human postmortem studies, all of limited scope (Standaert, 2011). Emerging data are challenging this view, however. The use of advanced neuroimaging techniques is identifying CNS microstructural abnormalities in human subjects, and recent rodent models exhibit degeneration during CNS maturation of discrete neuronal populations together with the appearance of abnormal twisting movements (Liang et al., 2014; Pappas et al., 2015; Ramdhani and Simonyan, 2013; Weisheit and Dauer, 2015).

One form of childhood-onset dystonia (DYT6) is caused by mutations in the gene coding for THAP1, an atypical zinc-finger transcription factor (Fuchs et al., 2009). Nearly 90 THAP1 mutations have been reported, including early (e.g., at amino acid 3) truncating mutations and a mutation that impairs dimerization (Sengel et al., 2011), essentially all of which are dominantly inherited (Blanchard et al., 2011; Houlden et al., 2010; Schneider et al., 2011). These data indicate that DYT6 mutations act by impairing THAP1 function. Diffusion tensor imaging implicates microstructural abnormalities of white matter in DYT6 subjects (Carbon et al., 2011; Cheng et al., 2012) and other forms of dystonia (Bonilha et al., 2007; van der Meer et al., 2012). The significance of these findings is uncertain, however, in part because THAP1 or other dystonia related genes have not been implicated in myelin biology. Indeed, very little is understood about THAP1 transcriptional targets or the molecular pathways in which it participates. Studies in human umbilical vein endothelial cells (HUVECs) suggest a role for THAP1 in cell-cycle regulation and apoptotic pathways (Roussigne et al., 2003). Similarly robust changes are not observed in THAP1 mutant murine brains (Ruiz et al., 2015), however, calling into question the relevance of cell-cycle-related events for THAP1 function in the CNS and for dystonia pathogenesis.

To define the normal role of THAP1 in the tissue and developmental context most relevant to disease pathogenesis, we used genetic strategies to explore the consequences of THAP1 loss-of-function in the developing CNS. Unbiased gene expression studies from motor regions of CNS-conditional THAP1 mutants demonstrated a specific pattern of transcriptional abnormality indicating a role for THAP1 in the control of myelination. Using *in vivo* and *in vitro* studies, we demonstrate that THAP1 plays a cell-autonomous role in oligodendrocytes (OL). THAP1

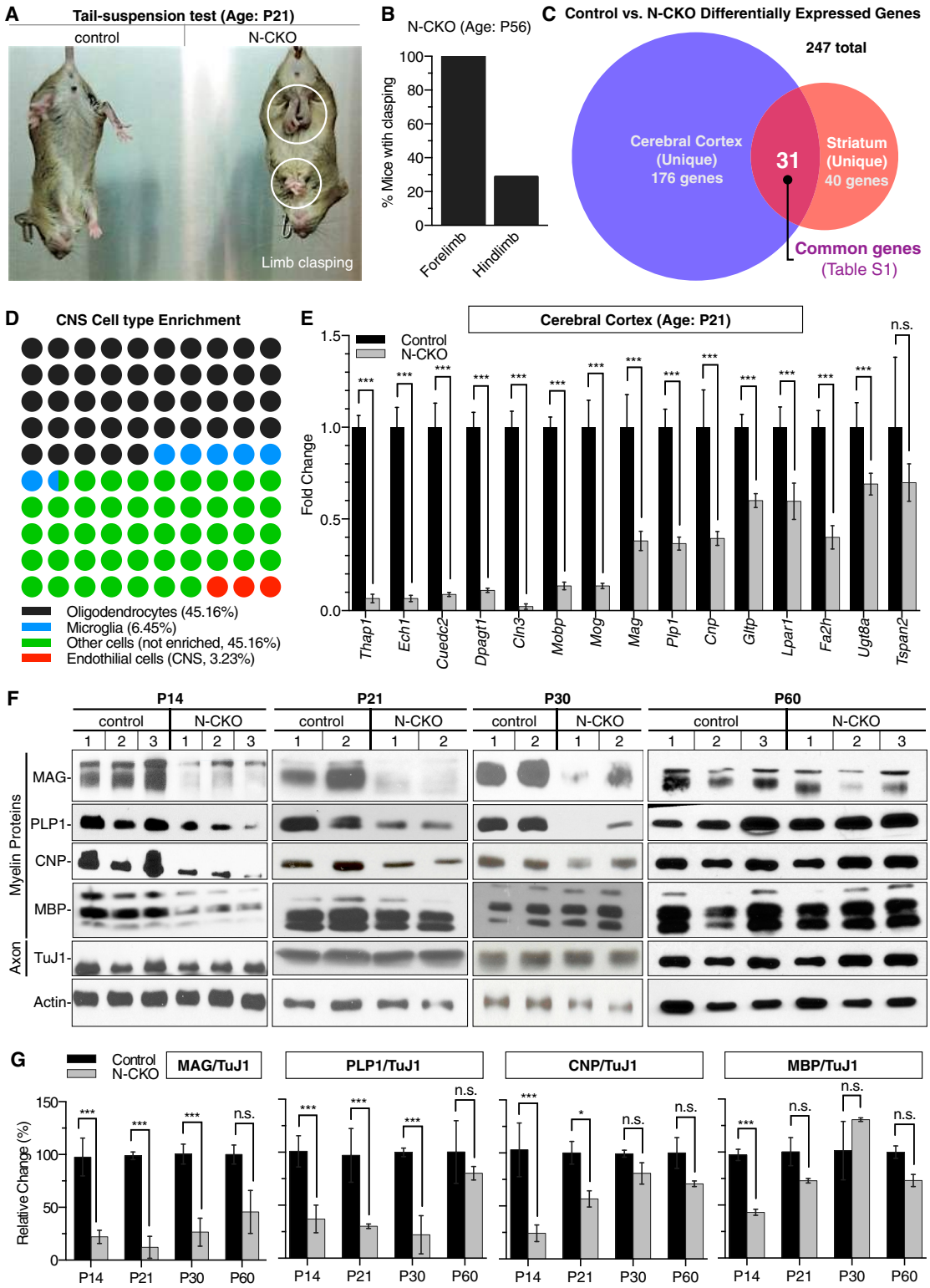

Figure 1. Conditional THAP1 Deletion from the CNS Causes Motor Deficits and Disrupts Myelination

(A and B) Juvenile N-CKO mice exhibit forelimb and hindlimb clasping during tail-suspension test. (A) Representative images of P21 N-CKO mice with forelimb and hindlimb clasping (circled in left image) and (B) quantitation of adult P56 N-CKO (*Thap1*$^{flx/-}$;nestin-*Cre*$^{+}$; n = 7) mice with forelimb and hindlimb clasping (represented as percentage; y axis). None of the control mice (*Thap1*$^{+/flx}$;nestin-*Cre*$^{+}$; n = 5) exhibited limb clasping.

(legend continued on next page)

deficiency delays the maturation of OL into myelin-producing cells without apparent effect on oligodendrocyte progenitor cells (OPC). Chromatin immunoprecipitation sequencing (ChIP-seq) studies demonstrate a striking cobinding on DNA of THAP1 with YY1, a transcription factor essential for OL lineage progression. Loss of THAP1 significantly impairs YY1 association at chromatin of THAP1-bound genes and, similar to YY1 loss of function, upregulates Id transcription factors that inhibit OL maturation. These data establish a functional relationship between these proteins and a mechanism for THAP1-related myelination defects. Considered together, these studies identify THAP1 as a transcriptional regulator of OL lineage progression, and provide a previously unrecognized molecular link between myelination and dystonia pathogenesis.

RESULTS

Conditional CNS Deletion of THAP1 Causes Motor Dysfunction and Deficient Myelin Gene Expression

Several DYT6 mutations impair THAP1 structure and/or function (Campagne et al., 2010; Ruiz et al., 2015; Sabogal et al., 2010; Sengel et al., 2011). To explore the consequences of THAP1 loss of function, we generated a floxed *Thap1* allele (*Thap1*^{flox}; deletion removes exons 2 and 3) that also contains the DYT6 F81L missense mutation (in exon 2; Fuchs et al., 2009), enabling a range of studies (Figure S1A). Mice heterozygous or homozygous for the F81L mutation did not exhibit any apparent differences in weight, life span, motor abnormality, or CNS pathology, indicating that the degree of THAP1 dysfunction caused by this mutation is not sufficient to generate overt abnormalities in the murine system (data not shown). We therefore explored the consequences of complete loss of function in THAP1, generating a germline null allele by intercrossing these mice with the Rosa-Cre line (Figure S1A) (Soriano, 1999). No *Thap1*$^{-/-}$ pups were recovered from intercrosses of these *Thap1*$^{+/-}$ mice. Previous reports indicate that germline deletion of *Thap1* causes embryonic lethality (Ortiz-Virumbrales et al., 2014; Ruiz et al., 2015). Consistent with this work, we found that *Thap1*$^{-/-}$ embryos were developmentally arrested by embryonic day 8.5 (E8.5) (Figure S1B). To circumvent the embryonic lethality, we conditionally deleted *Thap1* from the CNS by intercrossing nestin-*Cre* and *Thap1*^{flox} mice (herein THAP1 Nestin Conditional Knockout; N-CKO). THAP1 N-CKO mice were born in the expected Mendelian ratio (Figure S1C) and were indistinguishable from their littermate controls at birth. Molecular analyses confirmed that these mice are THAP1 deficient (Figures S1D and S1E). By approximately 3 weeks, N-CKO mice weighed ~25% less than their littermate controls (Figure S1F). N-CKO mice did not exhibit any spontaneous overt abnormal motor behaviors. Motor abnormalities similar to those reported previously (Ruiz et al., 2015) were present by 3 weeks of age, including abnormal limb clasping during tail suspension (Figure 1A and Movie S1). Retesting adult N-CKO mice at up to 2 months of age demonstrated that the limb-clasping phenotype is persistent (Figure 1B). At this time, they also exhibited significantly abnormal performance during beam crossing, and significantly increased rearing in the open field (Figures S1G–S1J). Considered together, these results demonstrate that THAP1 deficiency disrupts CNS maturation and causes persistent motor dysfunction.

To identify the molecular pathways that disrupt CNS maturation in N-CKO mice in an unbiased manner, we conducted global gene expression analyses on striatum and cortex, two brain regions central to motor control and strongly implicated in dystonia pathogenesis (Liang et al., 2014; Pappas et al., 2014, 2015; Tanabe et al., 2009). We performed microarray analyses comparing control and N-CKO RNA from these regions at postnatal day 21 (P21), the age when motor deficits are emerging (GEO: GSE97372). From a total of 71 differentially expressed genes in the striatum and 207 in the cortex, a core set of 31 genes was differentially regulated in both regions, 25 of which were downregulated (Figure 1C and Table S1). Strikingly, analysis of this core set of 31 genes using a cell-specific transcriptome database (Zhang et al., 2014) showed that ~45% are highly enriched in OL (>10-fold enrichment compared with other CNS cell types; Figure 1D) especially in maturing OL (Figure S1K). Strongly represented within this gene set were many myelin sheath constituents (*Cnp*, *Mag*, *Plp1*, *Mog*, *Mobp*, *Pllp*, and *Mal*) and genes normally upregulated in mature OL (*Lpar1*, *Fa2h*, *Gltp*, *Tmem63a*, *Zdhhc9*, and *Tspan2*). Downregulation of these genes was confirmed using qRT-PCR (Figure 1E). These molecular analyses implicated a role for THAP1 in myelination, a critical event during CNS maturation.

Myelination of the human and rodent brain is a largely postnatal process (Dean et al., 2015). In rodent, this process is mostly completed during the first month of life (Salmaso et al., 2014). To begin to explore whether myelination is disrupted in N-CKO mice, as indicated by the gene expression analyses, we first characterized the kinetics of myelination in wild-type animals from 2 weeks to 2 months of age (Figures S2A and S2B). All myelin proteins analyzed (CNP, MBP, MAG, PLP1, MOBP, and MOG) exhibited peak levels of expression at ~P21 (Figure S2B; myelin proteins normalized to total axonal content). THAP1 N-CKO mutants exhibited a profound reduction of several myelin proteins when analyzed over this same time frame. Consistent

(C) Summary of gene expression analyses from cortex and striatum of control (*Thap1*$^{+/flx}$;nestin-*Cre*$^{+}$; n = 4)) and N-CKO (*Thap1*$^{flx/-}$;nestin-*Cre*$^{+}$; n = 4) mice (Illumina BeadChip Array). The Venn diagram highlights a core set of 31 genes that were differentially regulated both in N-CKO cortex and striatum.

(D) Diagram illustrating the results of CNS cell-type specific transcriptome analysis (Zhang et al., 2014) demonstrating that 45% of the 31 genes dysregulated in N-CKO cortex and striatum are enriched (>10 fold) within the oligodendrocyte (OL) lineage.

(E) qRT-PCR analysis demonstrating the downregulation of candidate genes in N-CKO cortex. The RNA expression levels of *Thap1* and 14 candidate genes (normalized to ribosomal protein, *Rpl19*) from N-CKO (*Thap1*$^{flx/-}$;nestin-*Cre*$^{+}$; n = 4) cortex are represented as fold change with respect to their expression in littermate controls (*Thap1*$^{flx/+}$;nestin-*Cre*$^{+}$; n = 4). Graph shows mean values ± SEM. Significance values determined using t test: not significant (n.s.); ***p < 0.001.

(F and G) N-CKO mice exhibit significant reductions in several myelin protein components during juvenile CNS maturation. (F) Western blots of total forebrain homogenate and (G) corresponding quantitation for myelin component proteins (MAG, PLP1, CNP, and MBP), axon protein (TuJ1), and loading control (actin). The graph represents axon-normalized content (ratio of myelin/axon) for various myelin proteins as measured from intensity of the western blot (ImageJ analysis) and represented as a percentage change (y axis) to littermate controls (*Thap1*$^{flx/+}$;nestin-*Cre*$^{+}$) at ages P14, P21, P30, and P60. Graph shows mean values ± SEM. Significance values determined using t test: n.s., not significant; *p < 0.05, ***p < 0.001.

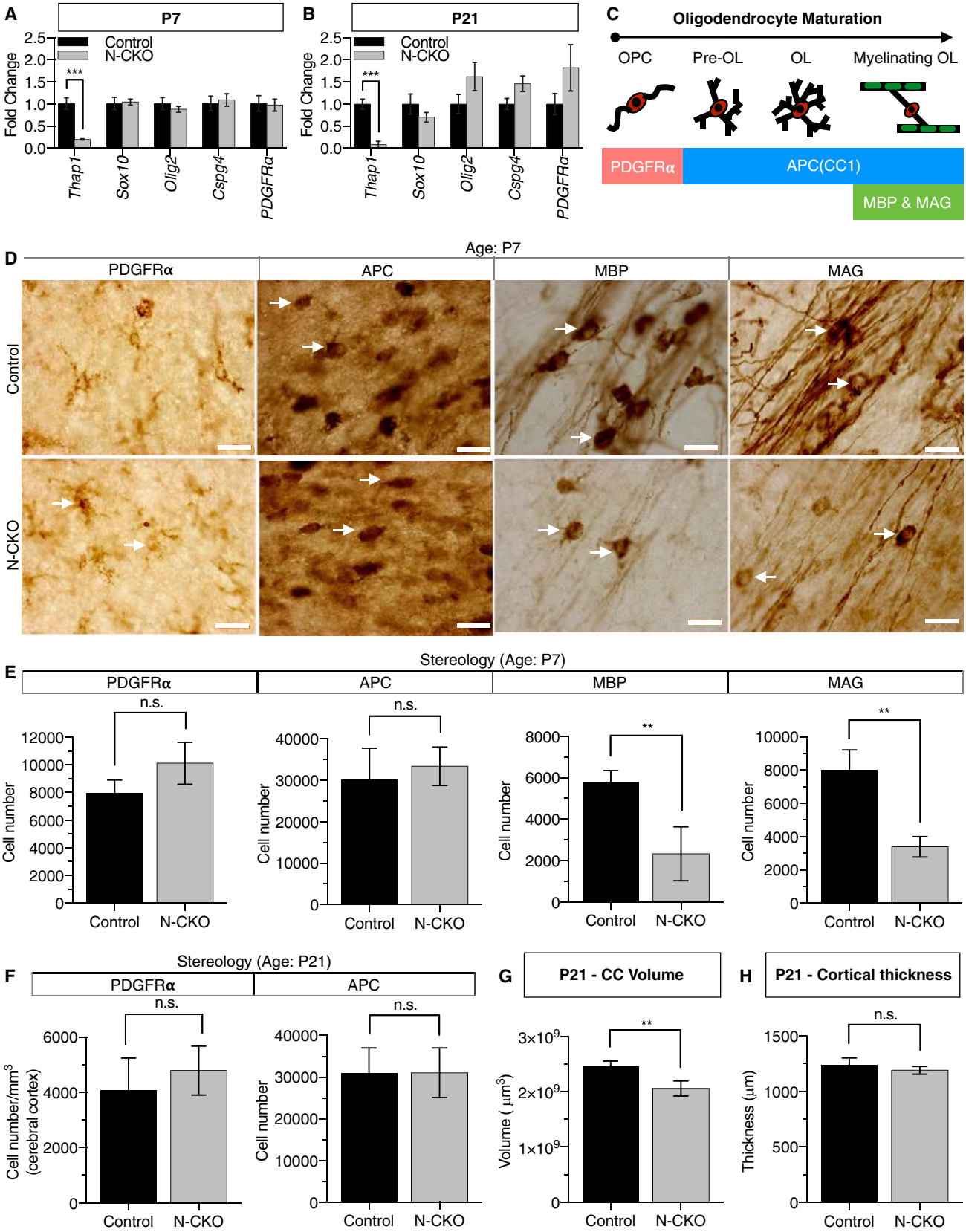

(legend on next page)

with the gene expression data, MAG and PLP1 protein levels (normalized to TuJ1 [tubulin β-III] levels) were significantly reduced (up to 5-fold) during the entire 4-week period (Figures 1F and 1G). Significant reductions were also observed for CNP (during the first 3 weeks) as well as for MBP (during the first 2 weeks). Notably, the levels of axonal marker TuJ1 (Figure S2C) did not decrease, suggesting that the abnormalities of myelin proteins arise from disrupted myelination per se, rather than from axon loss. Interestingly, the striking abnormality of myelination present during the first 3–4 weeks resolves by 2 months of age, at which time there are no significant differences between N-CKO mice and their littermate controls (Figures 1F and 1G). Thus, THAP1 deficiency appears to selectively disrupt myelination in the maturing CNS.

THAP1 Deficiency Impairs the Maturation of Progenitor Cells to Myelinating Oligodendrocytes

CNS myelination is a multistep process that includes the generation of OPC and their subsequent lineage development into mature OL, which then myelinate axons. Disruption of any of these steps could cause the defects observed in N-CKO mice. To begin to localize the defect responsible for the N-CKO myelination phenotype, we assessed OL lineage gene expression and quantified OL numbers at P7 and P21, ages representing the initiation and peak of postnatal forebrain myelination, and when clear defects in myelination exist in N-CKO mice. No changes were identified in the expression of "pan-OL" lineage genes (*Olig2* and *Sox10*) or those specifically expressed in OPC (*Cspg4* and *Pdgfr-2*) (Figures 2A and 2B). Similarly, normal numbers of OPC (identified by platelet-derived growth factor receptor α [PDGFRα]) were present in the corpus callosum (CC) of N-CKO mice, as assessed by unbiased stereology (Figures 2D–2F). These observations are consistent with the normal expression of OPC cell state-related genes in our microarray studies, indicate that OPC and OL numbers are normal in N-CKO mice, and suggest that THAP1 deficiency may impair later steps of OL maturation.

To assess OL maturation, we quantified OL lineage markers at P7 and P21 (Figure 2C). We first quantified the number of cells expressing MBP and MAG, markers characteristic of myelination-competent mature OL. At P7 there were significantly fewer MBP^+ and MAG^+ cells in the CC of N-CKO mice (MBP: 60% decrease, t test p = 0.0084; MAG: 58% decrease, t test p = 0.0011; Figures 2D and 2E). Estimating the number of MBP^+ or MAG^+ cells at P21 was not possible due to the presence of a dense MBP/MAG-expressing fiber network at this age. We therefore assessed the volume of MBP^+ fibers in the CC using the Cavalieri estimation (STAR Methods), identifying a significant (~30%) reduction in CC volume in N-CKO mice (t test p = 0.019; Figure 2G). In contrast to these abnormalities, no decrease was present at either age in the number of cells expressing "pan-OL" marker APC (CC1) that marks both immature and mature OL (Figures 2D–2F). Furthermore, we observed no changes in cortical thickness (average length from the dorsal boundary of the CC to the outer edge of cortical layer [STAR Methods]) in P21 mice with smaller CC volume, suggesting overall intact CNS structure (Figure 2H). Considered together, these analyses suggest that THAP1 impairs the maturation of OL but does not disrupt OPC generation.

THAP1 Deficiency Disrupts CNS Myelination via a Cell-Autonomous Effect in the Oligodendrocyte Lineage

The generation of myelinating OL and subsequent steps of myelination are highly regulated processes that involve extensive crosstalk between axons and OL. To determine whether the myelination defect in N-CKO mice arises from a cell-autonomous role of THAP1, we conditionally deleted *Thap1* from the OL lineage using Olig2-Cre mice (herein referred to as Olig2 Conditional Knockout; O-CKO). O-CKO mice were born in the expected Mendelian ratio and exhibited growth characteristics indistinguishable from their littermate controls (data not shown). Similar to N-CKO mice, at P21 O-CKO mice exhibit deficient expression of RNA and protein for all myelin components assessed (CNP, PLP1, MAG, MOBP; Figures 3A–3C). O-CKO mice also recapitulated the delay in OL maturation and reduced CC volume characteristic of N-CKO mice. At P7, we observed significantly fewer MBP^+ cells in the CC of O-CKO mice (control, 7,246 ± 785.8; O-CKO, 3,772 ± 385.8; t test p = 0.0041; Figures 3E and 3F). At P21, the O-CKO CC volume was significantly reduced (control, 2.65 ± 0.088 mm^3; O-CKO, 2.23 ± 0.11 mm^3; t test p = 0.011; Figure 3D). As with the N-CKO mice (Figure S3A), the deficiencies in the CC volume of juvenile O-CKO mice recovered in adult mice (Figure S3B). The myelination findings in O-CKO mice phenocopy those in N-CKO mutants,

Figure 2. THAP1 Deficiency Impairs the Ability of the Oligodendrocyte Lineage to Generate Mature Myelination-Competent Cells

(A and B) The expression of OPC-specific and pan-lineage genes is normal in N-CKO brain. qRT-PCR analysis of OPC-specific (*Cspg4*, *Pdgfr-2*) and pan-lineage genes (Sox10, Olig2) from (A) P7 and (B) P21 N-CKO (*Thap1*$^{flx/-}$;nestin-*Cre*$^+$; n = 3) cortex. RNA expression levels were normalized to *Rpl19* and are represented as a fold change relative to values from littermate controls (*Thap1*$^{flx/+}$;nestin-*Cre*$^+$; n = 3). Graph shows mean values ± SEM.

(C) Schematic showing the markers used to assess various OPC and OL populations.

(D–F) THAP1 deficiency impairs the generation of mature OL. Unbiased stereology was used to quantify cells expressing PDGFRα, APC, MBP, or MAG in the corpus callosum (CC) at P7 and P21 in control (*Thap1*$^{flx/+}$;nestin-*Cre*$^+$; n = 5) and N-CKO (*Thap1*$^{flx/-}$;nestin-*Cre*$^+$; n = 5) mice. (D) Characteristic images observed in quantifying the OL lineage. Images were acquired from the CC at 63× and cell counts quantified by an investigator blinded to genotype. Arrows highlight the representative cells counted in the images to obtain cell counts. Scale bar, 20 μm. (E and F) The number of OPC (PDGFRα) and post-OPC (CC1) cells (y axis) is normal in N-CKO tissue, but significantly fewer of these cells express markers characteristic of mature OL (MBP or MAG). PDGFRα counts for P21 mice were done in the cortex and represented as cell density (y axis). Graph shows mean values ± SEM.

(G) The CC volume is significantly reduced in N-CKO mice. Final volume of CC, as assessed using Cavalieri's estimator, is represented as μm^3 (y axis) for control (*Thap1*$^{flx/+}$;nestin-*Cre*$^+$; n = 5) and N-CKO (*Thap1*$^{flx/-}$;nestin-*Cre*$^+$; n = 5) mice (P21: control, 2.28 ± 0.08 mm^3; N-CKO, 1.92 ± 0.09 mm^3; p = 0.019, t test). Graph shows mean values ± SEM.

(H) N-CKO mice show no deficits in cortical thickness (P21: control, 1,237 ± 29.00 μm; N-CKO, 1,191 ± 15.48 μm; p = 0.20 (n.s., t test). Graph shows mean values ± SEM.

In the graphs, **p < 0.01 and ***p < 0.001; n.s., not significant.

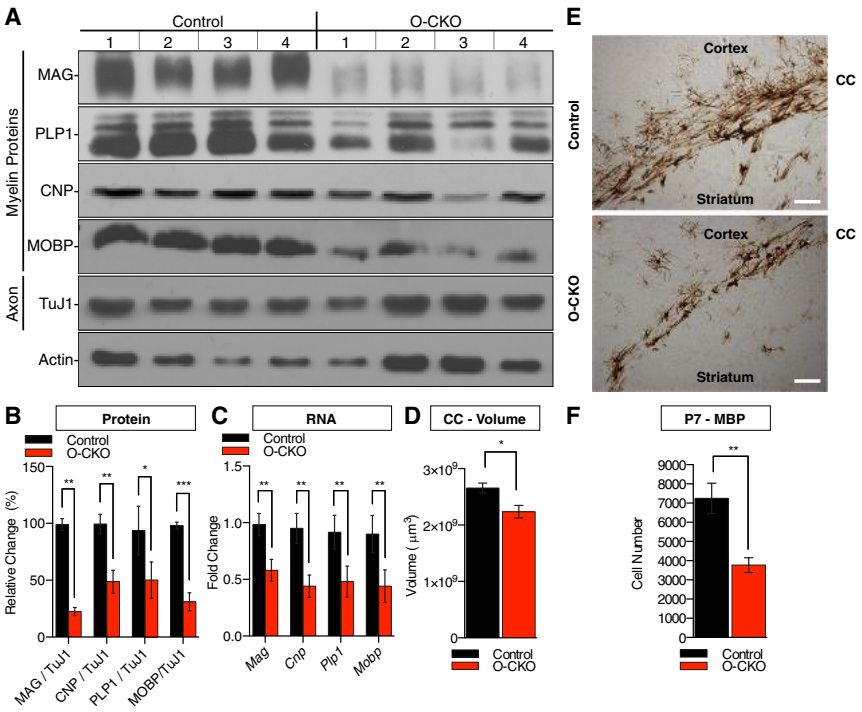

Figure 3. Conditional THAP1 Deletion from the Oligodendrocyte Lineage Disrupts Myelination

(A and B) Conditional deletion of THAP1 from OL lineage significantly reduces several myelin protein components. *Thap1* floxed mice were intercrossed with Olig2-Cre mice (Olig2-Cre Conditional Knock Out, "O-CKO") to selectively delete THAP1 from the OL lineage. Western blot analyses (P21) of forebrain homogenates for myelin (MAG, PLP1, CNP, and MOBP), axon proteins (TuJ1) and loading controls (ACTIN). The graph (B) shows quantification of the western blots, with myelin/axon ratio after normalization to the loading control (Actin) and represented as a percentage change (y axis) to littermate controls ($Thap1^{flx/+}$;nestin-Cre^{+}) at the age of P21. Graph shows mean values ± SEM.

(C) qRT-PCR analysis confirming the RNA down-regulation of the candidate OL genes in THAP1 O-CKO cortex ($Thap1^{flx/flx}$;Olig2-Cre^{+}; n = 4). RNA expression levels are normalized to ribosomal protein *Rpl19* and represented as fold change compared with littermate controls ($Thap1^{flx/+}$;nestin-Cre^{+}; n = 4). Graph shows mean values ± SEM.

(D) The volume of O-CKO mice is significantly smaller that littermate controls. Final volume of CC, as assessed using Cavalieri's estimator, is represented as μm^3 (y axis) for control ($Thap1^{flx/+}$;nestin-Cre^{+}; n = 5) and O-CKO ($Thap1^{flx/flx}$;Olig2-Cre^{+}; n = 5) P21 mice. Control, 2.65 ± 0.088 mm^3; N-CKO, 2.23 ± 0.001 mm^3; p = 0.01, t test). Graph shows mean values ± SEM.

(E and F) Conditional deletion of THAP1 from OL lineage impairs the generation of mature OL. Unbiased stereology was used to quantify cells expressing MBP in the corpus callosum (CC) at P7 in control ($Thap1^{+/+}$; n = 5) and O-CKO ($Thap1^{flx/lx}$;Olig2-Cre^{+}; n = 5) mice. (E) Representative images (scale bar, 100 μm) and (F) number of MBP^{+} cells (y axis) is significantly decreased in the CC of the O-CKO tissue. Graph shows mean values ± SEM.

In the graphs, significance values determined using t test: *p < 0.05, **p < 0.01, ***p < 0.001.

indicating a cell-autonomous role for THAP1 in OL maturation *in vivo*.

To further examine the role of THAP1 in CNS myelination, we used electron microscopy (EM) to assess nerve fiber ultrastructure in N-CKO and O-CKO mice. We assessed the percentage of myelinated axons and myelin thickness (G ratio) in optic nerve (ON) and the genu of the CC. We began by comparing N-CKO and O-CKO mice at P21, the age of most of our prior biochemical, genetic, and behavioral studies. Both lines of mice exhibit severe hypomyelination but no abnormality in the number or morphology of axons (Figures 4A–4D). At this age, both lines of mice exhibited a roughly 5-fold decrease in the number of myelinated CC axons (Figures 4A and 4B). Similarly, both lines of mice exhibited a roughly 2-fold decrease in the number of myelinated ON axons (Figures 4C and 4D). Despite severe hypomyelination, the density of total axons (myelinated and non-myelinated combined) was normal in both lines (Figures 4B and 4D). We further assessed nerve cell integrity in N-CKO mice by quantifying the density of the retinal ganglion cell bodies that give rise to ON axons, finding no significant difference (Figure S3C). Normal axon number is consistent with our western blot analyses using TuJ1 in both N-CKO and O-CKO brain homogenates (Figures 1G and S2C).

Having confirmed that the myelination defects in N-CKO mice are mimicked by conditional deletion of *Thap1* in oligodendrocytes, we examined the changes in myelin ultrastructure with age in O-CKO mice. At P14, the defects in CC and ON appear similar to those present at P21 (Figures 4B, 4D, 4E, and 4H). The differences in CC were not significantly different, however, likely because very few control axons are myelinated in CC at this early age. Consistent with the adult recovery of myelin proteins in N-CKO mice (Figures 1F and 1G), we observed a complete recovery in the percentage of myelinated axons in ON, and a far less dramatic difference in CC (from a ~5-fold decrease at P21 to a ~35% decrease at 1 year; Figures 4E and 4H).

For myelinated axons, we also assessed the formation of compact myelin by measuring G ratio (ratio of the inner axonal diameter to total diameter including myelin) in juvenile and adult mice. In contrast to the marked differences in the percentage of axons myelinated, we observed modest (but in some cases significant) changes in G ratio. At our P21 reference age, both O-CKO and N-CKO mice show statistically significant changes in myelin thickness in CC (Figures 4F and S3D). At this age in ON, there are small but significant differences for O-CKO mice but not for N-CKO mice (Figures 4I and S3E). At 1 year of age, subtle changes in myelin thickness (~5% higher G ratio) persist in CC, but not ON, in O-CKO mice (Figures 4G and 4J). Considered together with the profound differences in the percentage of myelinated axons in juvenile mice and the normal numbers of OPC- and CC1-positive OL, these data are most consistent with a key role for THAP1 in OL maturation and myelination initiation during postnatal CNS development, rather than on the formation of compact myelin. The striking similarity of these measures in N-CKO and O-CKO mice strongly supports the likelihood that these effects arise from a cell-autonomous role of THAP1 in the OL lineage.

THAP1 Loss Impedes the Maturation of Purified Oligodendrocyte Cells

To more rigorously explore the possibility of cell-autonomous THAP1 effects, we tested whether similar defects exist when the OL lineage is examined in isolation *in vitro.* We purified three independent lines of neural stem cells (NSC) each from wild-type and O-CKO mice, and generated OPC from these lines (Figure 5A and STAR Methods). Immunocytochemistry (ICC) and gene expression analyses for markers of NSC (*Pax6* and *Nestin*) demonstrated that NSC cells isolated from wild-type and O-CKO mice have similar characteristics (Figures S3F–S3H). The OPC cells derived from the NSC lines were positive for SOX10/OLIG2/CSPG4(NG2)/PDGFRα (>95%) and were maintained as such in a PDGF/fibroblast growth factor 2 (Fgf2)-dependent manner (Figure S3I and STAR Methods). Further analyses in control and O-CKO OPC using pan-OL and OPC lineage markers (*Cspg4,Pdgfr-2*, *Olig2*, and *Sox10*) by ICC and gene expression analysis demonstrated that wild-type and mutant OPC lines exhibited comparable expression of all relevant markers (Figures S3I and S3J). The ability to derive and maintain THAP1 null OPC from NSC *in vitro* is consistent with our observations *in vivo* indicating that THAP1 deficiency does not disrupt OPC generation or maintenance (Figure 2).

We next tested whether progression of OPC to early OL occurred normally in *Thap1* null cultures, as appears to be the case *in vivo* (Figure 2). Driving OPC down the OL lineage (by changing them into OPC differentiation media [ODM] devoid of PDGF and Fgf2; STAR Methods) demonstrated that a similar percentage of wild-type and O-CKO OPC progressed to CNPase-expressing cells (Figures 5B–5D) and developed bipolar processes characteristic of the OL lineage (Figure S3I). THAP1 deficiency has been linked to a defect in cell-cycle exit (Cayrol et al., 2007), an event critical for OL lineage progression. However, THAP1 null OPC appeared similar in their ability to exit the cell cycle and to progress beyond the progenitor state, as evidenced by the similarly rapid decreases (~10-fold) in RNA of an OPC-specific marker Cspg4 and cell-cycle markers previously implicated in THAP1 biology in cell culture (*E2f1* and *Cdc2*; Figure 5F). These *in vitro* data are consistent with findings *in vivo*, and indicate that THAP1 deficiency does not disrupt the progression of OPC to early OL.

Similar to observations *in vivo*, THAP1 null cultures exhibited significant abnormalities of later events characteristic of OL lineage progression. By day 6 of PDGF withdrawal from O-CKO cultures, ~50% fewer MBP^+ cells were generated compared with control cultures (wild-type, 56.25% ± 7.5%; KO, 28.25% ± 2.76%; chi-square $p < 0.001$; Figures 5B and 5E). A similar defect of maturation to the MBP-expressing stage was also observed when the OPC were treated with triiodothyronine (T3), another widely used maturation paradigm (wild-type, 81.6% ± 5.4%; KO, 44.6% ± 7.23%; chi-square $p < 0.001$; Figures 5C and 5E). Moreover, even in those O-CKO cells that did express MBP, staining intensity was significantly reduced (MBP intensity represented as a.u.: control, 388.8 ± 5.7 a.u.; O-CKO, 268.8 ± 3.466 a.u.; t test $p < 0.001$; Figure 5G). The overall area covered by O-CKO OL processes, another indicator of maturation, was also significantly reduced (frequency distribution; Figure 5H; average size of MBP^+ OL for control = 3,831 ± 107.1 μm^2 and for O-cKO = 3,246 ± 167.4 μm^2; t test $p = 0.0023$). The expression of OL maturation-related genes was also defective in O-CKO cultures. We measured the expression of the set of 11 OL-enriched genes altered by THAP1 loss in both cortex and striatum (Table S1 and Figure 1). During differentiation of OPC to OL, in THAP1 null cultures, eight of these OL-enriched genes were significantly reduced (*Mbp*, *Mag*, *Plp1*, *Mog*, *Ugt8a*, *Tmem63a*, *Tspan2*, and *Cnp*), one was significantly increased (*Pllp*), and two were unchanged (*Gltp* and *Fa2h*) (two-way ANOVA with Sidak's post hoc test, $p < 0.001$; Figures 5I, 5J, and S3K). Notably, THAP1 appears to be essential for the expression of *Mobp* in the developing OL lineage, as this gene was essentially uninduced in differentiated THAP1 null cultures (Figure 5I). Use of the T3 differentiation paradigm yielded similar differences, with the exception of *Ugt8a*, which exhibited a normal expression pattern in this paradigm (Figure 5J). These observations, considered together with multiple lines of evidence *in vivo*, firmly establish a cell-autonomous role for THAP1 in the maturation of OL to myelin-producing cells, and indicate that most or all of the gene expression changes observed in N-CKO mice arise from the action of THAP1 within the maturing OL lineage.

Consistent with the role of THAP1 specifically in mature OL, we see no change in the expression of immature OL marker *Ennp6* (Figure S3K) (Xiao et al., 2016). Interestingly, we observed no significant difference in the expression of the pro-maturation *Myrf* in OPC up to 2 days following PDGF withdrawal during the early period of OL induction (Figure S3K; *Myrf* was induced in both lines by ~30-fold). Thus, robust *Myrf* activation can occur in the absence of *Thap1.* In more mature cells, 4 days following T3 treatment, we did observe significantly decreased *Myrf* levels, a pattern similar to that seen in other myelin component genes (Figure S3K). Based on these data, we believe that the impact of *Thap1* loss occurs independently of (and despite the expression of) *Myrf.* The broad consistency of findings between the *in vitro* studies in a purified OL lineage and those in N-CKO mice (Figure 1) validate the use of this culture system for mechanistic studies of THAP1 function relevant to its CNS role and DYT6 dystonia pathogenesis.

THAP1 Colocalizes with and Affects the Occupancy of YY1 in Oligodendrocytes

THAP1 is expressed ubiquitously both regionally and developmentally in rodents, including broadly in CNS cell populations (Figures S4A and S4B). This broad expression pattern suggests that THAP1 requires cofactors to engage with OL maturation pathways. We pursued a multistep bioinformatics approach to define a set of THAP1 candidate cofactors (Figure 6A). Essential to this effort was a publicly available THAP1 ChIP-seq dataset (GEO: GSM803408). Notably, nearly three-quarters of the 2,471 THAP1-associated binding peaks in this database were localized within 1 kb of the transcription start site (TSS; Figure S4C). We first identified which of the 247 genes dysregulated in *Thap1* null cortex or striatum (Figure 1C and Table S1) are bound directly by THAP by comparing them with the THAP1 ChIP-seq dataset. This analysis yielded a group of 44 genes, herein referred to as THAP1-CNS genes (Table S2).

We next pursued two analyses to identify proteins and transcription factors with binding motifs significantly enriched at these THAP1-CNS genes, and compared these results to

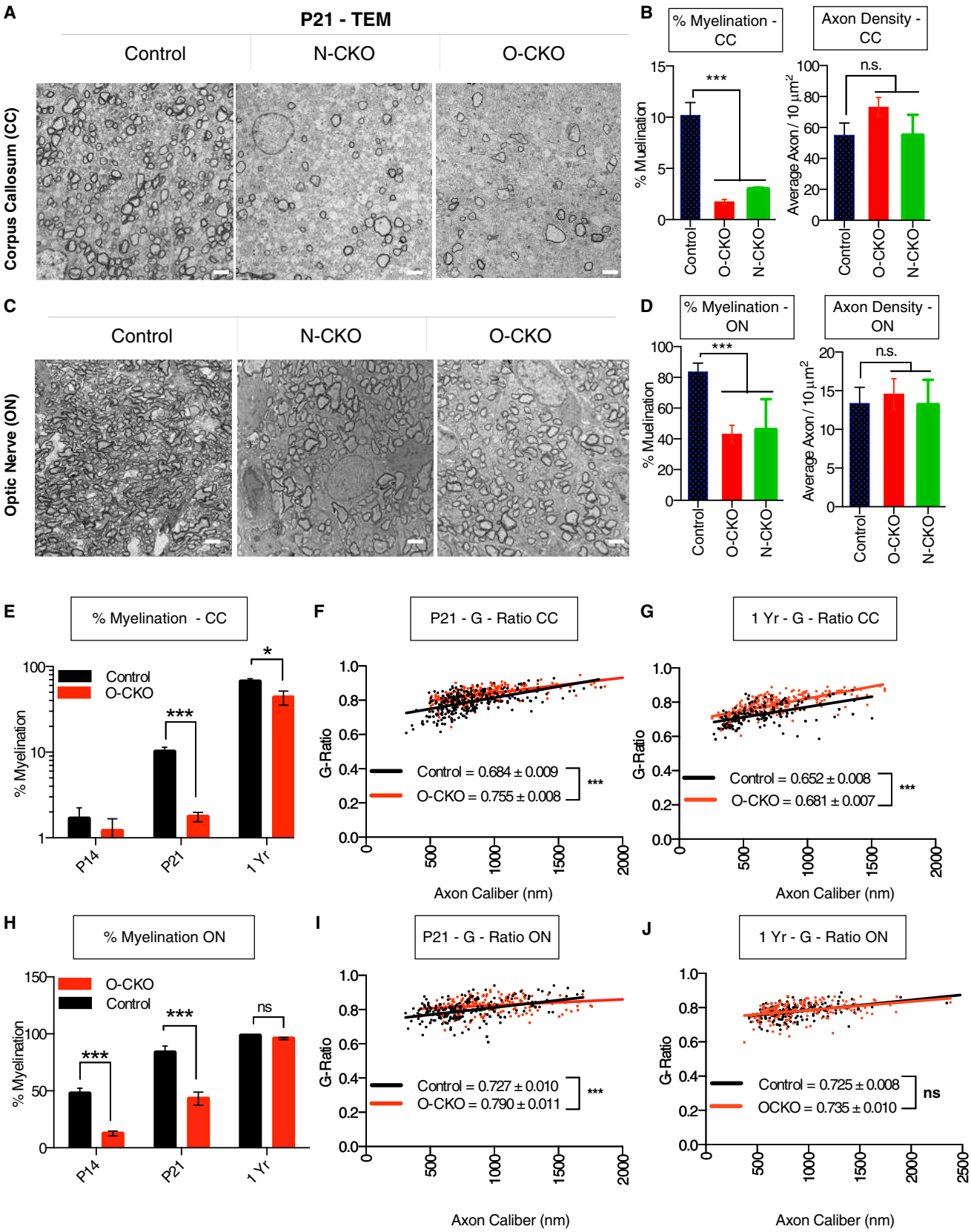

(legend on next page)

identify likely THAP1 cofactors (Figure 6A). The ENCODE ChIP-seq significance tool (Auerbach et al., 2013) identified 70 proteins significantly enriched at >50% of THAP1-CNS genes (hypergeometric test; Benjamini-Hochberg $p < 10^{-2}$) from either human or mouse genome (Table S3). As expected, this list included elements of the core transcription machinery such as PolII, TAF, and TBP in addition to transcription factors. Analysis using the Distant Regulatory Elements (DiRE) tool (Gotea and Ovcharenko, 2008) yielded 120 transcription factors with significantly enriched binding motifs at THAP1-CNS genes (Table S4). Comparison of these analyses yielded eight genes in common (Table S5). Of these, among the most statistically significant and biologically notable was the transcription factor YY1, which has an established role in OL maturation (He et al., 2007). YY1 had the highest score for "transcription factor importance" in the DiRE analysis and was among the most significantly enriched proteins in the ENCODE ChIP-seq analysis (hypergeometric test; Benjamini-Hochberg $p = 5.4 \times 10^{-9}$), binding 39 of the 44 THAP1-CNS genes (Table S5).

To examine a potential relationship between THAP1 and YY1 more broadly, we examined the overlap of their respective ENCODE ChIP-seq datasets (YY1; GEO: GSM803446). Strikingly, roughly 97% of all THAP1-bound genes were also bound by YY1, further supporting the possibility of a functional relationship between these transcription factors (Figure S4D; data from K652 cells). Having observed a significant overlap in the genome-wide localization of THAP1 and YY1, we tested whether these proteins coassociate. Exogenously expressed FLAG-tagged THAP1 (FLAG-THAP1) and YY1 coimmunoprecipitate in HEK293 cells, demonstrating coassociation of these proteins (Figure 6C). We did not detect coimmunoprecipitation of endogenous YY1 by THAP1 and vice versa (Figure 6C), however, suggesting that the observed association of THAP1 and YY1 is a weak or low-stoichiometric event.

To test more directly for a functional relationship between these proteins in the context of gene regulation, we used ChIP to assess YY1 DNA occupancy in wild-type and *Thap1* null cells. These analyses were performed on chromatin isolated from OL cells differentiated for 2 days by T3 treatment of OPC cells, and on embryonic stem cells (ESC), the rapid division of which enabled us to isolate sufficient quantities of material for analysis. We examined four sets of genes: (1) five candidate genes (*Ech1*, *Cuedc2*, *Prepl*, *Tmem180*, and *Dars2*) that ENCODE data indicate have THAP1 and YY1 binding peaks at the same genomic locations (Figure 6B); (2) five genes (*Rpl13a*, *Raptor*, *Fbxo28*, *Mynn*, and *Ncstn*) to which YY1 but not THAP1 is predicted to bind; (3) genes (*Cnp*, *Plp1*, *Mag*, *Mog*, *Ugt8a*, and *Mobp*) coding for myelin components that are downregulated in *Thap1* null differentiating OL; and (4) two active genes (*Gapdh* and *Hprt*) predicted not to be bound by THAP1 or YY1 (Figure 6B). We confirmed THAP1 and YY1 bind specifically at all predicted candidate genes (Figures 6D–6G, S5A, and S5B) in both OL cells and ESC. The specificity of the antibody for THAP1, the same used for the ENCODE ChIP-seq experiment, was confirmed by the near complete absence of signal with this antibody on chromatin from *Thap1* null cells (Figures 6D–6G, S5A, and S5B) and negligible signal with use of an isotype-specific control antibody (goat immunoglobulin G [IgG]) (Figure 6D). The specificity of the YY1 binding was confirmed by demonstrating negligible signal with use of an isotype-specific control antibody (rabbit IgG) (Figure 6E). In contrast to YY1 binding at all five candidate genes tested on chromatin from wild-type cells, binding of YY1 was markedly and significantly reduced at all these genes on chromatin from *Thap1* null OL cells and ESC (Figures 6F, 6G, S5A, and S5B). Consistent with the specificity of these effects, there was no significant change in YY1 occupancy in *Thap1* null cells at the five genes predicted to have YY1 but not THAP1 occupancy (Figures 6F, 6G, S5A, and S5B). THAP1 and YY1 both associate with the TSS of *Thap1* gene, further indicating a functional relationship between these proteins (Figures S5C). THAP1 was not bound to the *Yy1* locus (data not shown) and we observed no change in the expression of *Yy1* in *Thap1* null OPC, or differentiating OL (Figure 6H). These data suggest that THAP1 loss affects YY1-related genes through occupancy at shared loci, not by altering the expression of YY1. Interestingly, no THAP1 or YY1 binding was observed at any of the six myelin genes tested in OL cells or ESC (Figures 6F, 6G, S5A, and S5B). We found no binding at these myelin genes despite testing multiple THABS regions within each of these genes in OL cells and ESC (data not shown). These data suggest that THAP1 (and YY1) regulate myelin genes through an indirect mechanism.

Two potential mechanisms have been advanced to explain the role of YY1 in myelin gene regulation: (1) YY1 is a regulator

Figure 4. CNS Structural Defects in THAP1-Deficient Mice

(A–D) Significantly fewer axons are myelinated in N-CKO and O-CKO CNS. (A and C) Representative EM images of control (*Thap1*$^{+/+}$;nestin-*Cre*$^{-}$; n = 5), N-CKO (*Thap1*$f^{lx/-}$;nestin-*Cre*$^{+}$; n = 5), and O-CKO (*Thap1*$^{flx/lx}$;Olig2-*Cre*$^{+}$; n = 5) from (A) CC (Genu) and (C) ON at P21, demonstrating significantly higher number of unmyelinated axons in *Thap1* mutants. Scale bar, 2 μm. (B and D) The percentage of axons myelinated (y axis) was quantified by counting more than 1,000 axons from control, O-CKO, and N-CKO from CC (control, 10.16% ± 1.276%;, O-CKO, 1.762% ± 0.218%; N-CKO, 2.98% ± 0.072%; $p < 0.0001$, chi-square) and ON (control, 83.76 ± 5.51; O-CKO, 43.09 ± 5.76; N-CKO, 45.96 ± 9.95; $p < 0.001$, chi-square). There is no decrease in axon density (y axis; axons/10 μm^2) in both O-CKO and N-CKO mice relative to control in CC (control, 55.16 ± 7.81; O-CKO, 73.28 ± 6.121; N-CKO, 54.89 ± 6.67) and ON (control, 13.39 ± 2.04; O-CKO, 14.56 ± 1.99; N-CKO, 13.19 ± 1.01). Axon density was measured as total number of axons (myelinated and non-myelinated) estimated from ten individual images (obtained at 4,000× magnification). Graph shows mean values ± SEM.

(E and H). Significantly fewer axons are myelinated in juvenile O-CKO CNS compared with adult. The percentage of axons myelinated (y axis) was quantified from control and O-CKO in (E) CC and (H) ON from ages P14, P21, and 1 year. Note that the P21 data for (E) and (H) are reproduced in (B) and (D) for clarity of age-based comparisons. Graph shows mean values ± SEM.

(F, G, I, and J) Characterization of myelin thickness in *Thap1* null CNS. The G ratio (ratio of the inner axonal diameter to total [including myelin] outer diameter) for control and O-CKO mice at ages P21 from (F) CC (control, 0.684 ± 0.009; O-CKO, 0.7550 ± 0.008; $p < 0.0001$, t test) and (I) ON (control, 0.727 ± 0.010; O-CKO, 0.790 ± 0.011; $p < 0.0001$, t test). Also shown in the figure are the G ratio for 1-year-old mice from (G) CC (control, 0.652 ± 0.008; O-CKO, 0.681 ± 0.007; $p < 0.0001$, t test) and (J) ON (control, 0.725 ± 0.008; O-CKO, 0.735 ± 0.010; $p = 0.545$, t test).

In the graphs, *$p < 0.05$ and ***$p < 0.001$; n.s., not significant.

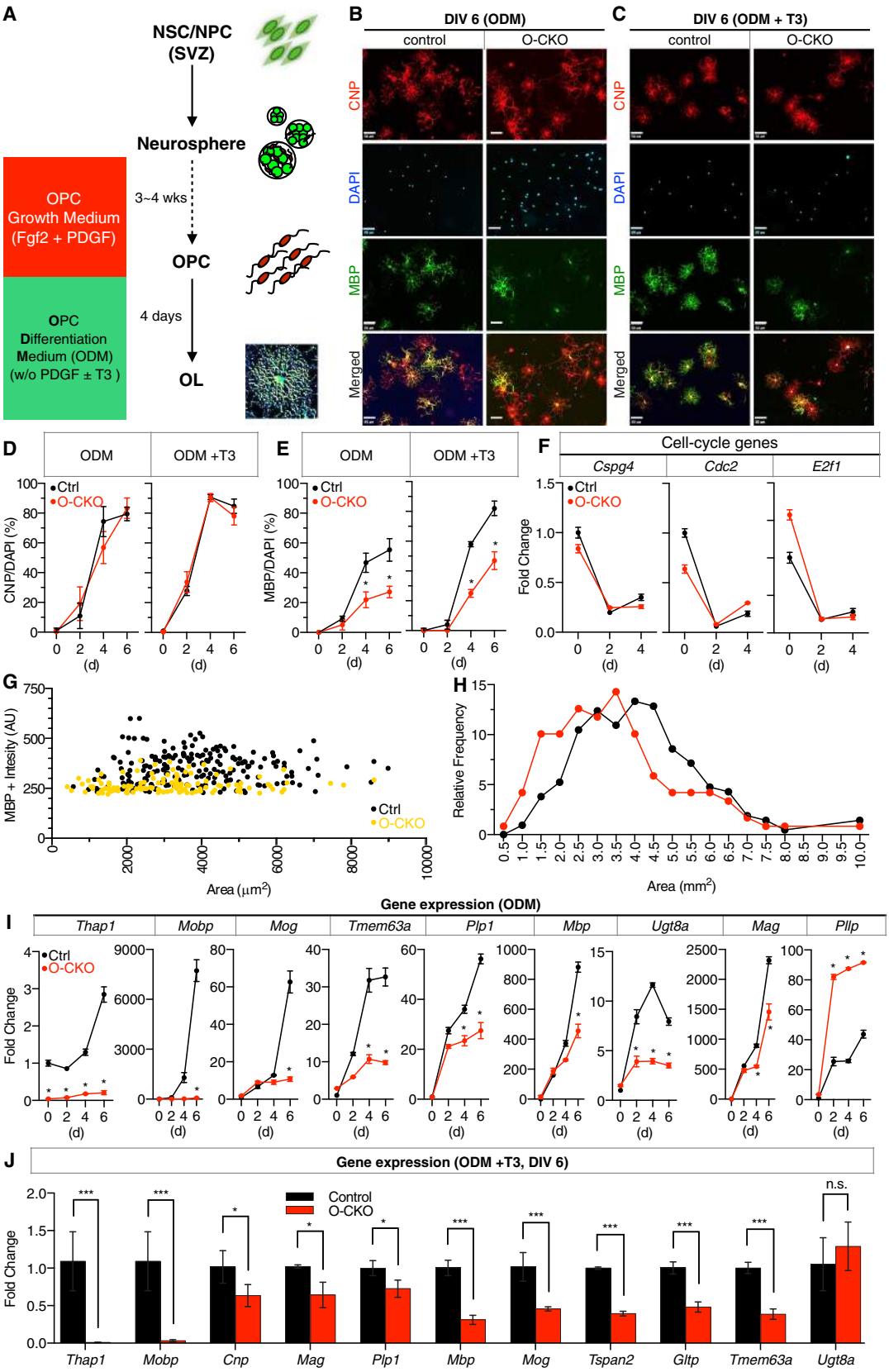

(legend on next page)

of *Plp1* expression (Berndt et al., 2001; Heng et al., 2013; Zolova and Wight, 2011); and (2) YY1 suppresses Id genes (*Id2* and *Id4*) and *Tcf4* in OL by recruiting HDAC1 (He et al., 2007), thereby facilitating the maturation of OL cells. We explored whether these mechanisms may help explain the consequences of *Thap1* loss for myelination. We tested for THAP1 and YY1 binding at multiple predicted binding sites in *Plp1*: (1) promoter, (2) putative THAP1 binding sites, and (3) ''ASE'' (anti-silencer/enhancer), an intronic regulatory site reported to be responsible for YY1-mediated repression of *Plp1* (Zolova and Wight, 2011). We detected no THAP1 or YY1 binding at any of these sites in OL (Figures 6F and 6G). We did observe significantly increased YY1 binding at ASE in *Thap1* null OL (Figures 6F and 6G), but the magnitude of binding was near that of IgG control and therefore quantitatively negligible compared with any of the regions with confirmed YY1 association (Figures 6F and 6G).

In contrast to our results with *Plp1*, we found the Id genes (*Id2*, *Id4*) to be robustly upregulated in *Thap1* null OL, paralleling observations made for *Yy1* loss (He et al., 2007) (Figure 6H). While Id gene upregulation in *Thap1* null OL mimics observations made following YY1 loss of function, we do not observe significant changes in the expression of *Tcf4* or other Wnt pathway genes tested (*Tcf4*, *Axin2*, and *Wnt3a*) (Figure 6H). Unlike that report, however, we observe no significant binding of YY1 to either of the *Id* loci in OL (Figure 6G). We did detect YY1 occupancy at *Id4* in ESC, however, which was significantly reduced by the loss of THAP1 (Figure S5B). The absence of YY1 binding to *Id2* and *Id4* in OL is unlikely to be a methodological issue, as we detect robust YY1 occupancy at ten other loci in these cells previously reported to be YY1 bound (Figures 6G and S5B). We also failed to detect evidence of decreased HDAC occupancy in *Thap1* null cells (Figure S5D), previously suggested as a mechanism of *Id* or *Tcf4* gene regulation in YY1-deficient cells (He et al., 2007). Considered together, however, these data clearly establish a functional relationship between THAP1 and YY1, and advance a mechanistic model of the relationship between THAP1 and key developmental pathways regulating OL development and myelination.

DISCUSSION

Our studies establish THAP1 as a participant in pathways controlling the inception of myelination during CNS maturation. A cell-autonomous role for THAP1 in the OL lineage is supported by transcriptional, protein, histological, and ultrastructural studies *in vivo*, as well as complementary studies *in vitro.* Consistent with these findings, we link THAP1 to the transcription factor YY1, a molecule with an established role in myelination control. We identify a striking overlap between THAP1- and YY1-bound genes, demonstrate that loss of THAP1 significantly impairs YY1 DNA occupancy, and find that similar to *Yy1* loss, *Thap1* loss causes upregulation of Id gene mRNAs. These are the first studies to link a genetic cause of primary dystonia to myelination pathways and, considered together with Diffusion tensor imaging studies in human subjects with DYT6 and other forms of dystonia, implicate abnormal timing of myelination in the pathogenesis of dystonia (Carbon et al., 2011; Bonilha et al., 2007; van der Meer et al., 2012). A recent report of progressive dystonia in subjects with YY1 haploinsufficiency further strengthens the link between YY1, THAP1 and dystonia (Gabriele et al., 2017).

There are nearly 90 DYT6-associated mutations reported for THAP1, including early truncation mutations (e.g., at amino acid 3; Q3X), strongly supporting a loss-of-function mechanism of disease pathogenesis (Blanchard et al., 2011). Consistent with the clinical genetic data, direct experimental evidence demonstrates that the pathogenic C54Y mutation impairs THAP1 function *in vivo* (Ruiz et al., 2015). This mutation, which occurs within the DNA binding domain, phenocopies the embryonic lethality of *Thap1* null mice (both $Thap1^{C54Y/-}$ and $Thap1^{C54Y/C54Y}$ exhibit early embryonic demise) (Ruiz et al., 2015). Our finding of early embryonic lethality consequent to germline *Thap1* ablation is consistent with this and another report (Ortiz-Virumbrales et al., 2014), but the F81L mutation did not exhibit any overt effects at the organismal level. While nearly all of the DYT6 mutations are dominantly inherited, two (L32H and N136S) are recessively inherited, indicating that mutations differ in the extent to which they impair *THAP1* function. These observations indicate that the F81L mutation impairs THAP1 less than the C54Y

Figure 5. THAP1 Plays a Cell-Autonomous Role in the Oligodendrocyte Lineage

(A) Schematic of the protocol used to derive OPC and its differentiation into mature OL from THAP1 null ($Thap1^{Flx/Flx}$;Olig2-Cre^{+}) and control ($Thap1^{+/+}$) SVZ-derived neural stem cells (NSC).

(B–H) THAP1-deficient OPC show deficits in OL maturation. (B and C) Images of MBP/CNP staining for control ($Thap1^{+/+}$) and THAP1 null OPC ($Thap1^{Flx/Flx}$;Olig2-Cre^{+}) cells differentiated by PDGF withdrawal (ODM) without (B) or with T3 addition (C) for 6 days. Scale bar, 50 μm. (D) Quantification of CNP-expressing OL differentiated days 0 through 6 (x axis) following PDGF withdrawal without or with T3 addition. (E) Quantification of mature MBP-expressing OL (CNP-expressing) differentiated days 0 through 6 (x axis) following PDGF withdrawal without or with T3 addition. Graph shows mean values ± SEM. Asterisks represent time points where significant differences exist using Sidak's post hoc multiple comparison test. (F) *Thap1* null OPC show no deficits exiting the cell-cycle and progenitor cell state. qRT-PCR analysis for candidate cell-cycle genes (Cdc2, E2f1) and an OPC-specific marker (*Cspg4*). (G) Scatterplot of MBP staining intensity (measured by ImageJ and represented as a.u. Control, 388.8 ± 5.78 a.u.; O-CKO, 268.8 ± 3.466 a.u.; $p < 0.001$, t test) for *Thap1* null (yellow) and control (black) OL. (H) Frequency histogram of the areas of mature (MBP-expressing) OL from THAP1 null (red) and control OL (black) cultures. The average area covered by MBP-stained OL in THAP1 null is smaller than that by control cultures (data not shown; control, 3,831 ± 107.1 μm^2; O-cKO, 3,246 ± 167.4 μm^2; $p = 0.0023$, t test).

(I and J) Deficient expression of OL-enriched THAP1-CNS genes during OL differentiation. (I) qRT-PCR is depicted for multiple days following PDGF withdrawal. Gene expression values are normalized to Olig2 expression and represented as fold change compared with day-0 OPC values. Graph shows mean values ± SEM. Two-way ANOVA demonstrates a main effect of genotype ($p < 0.01$) for all genes shown in panel I. Asterisks represent time points where significant differences exist using Sidak's post hoc multiple comparison test. (J) Similar transcriptional defect in myelin program genes during differentiation protocol including T3 addition. qRT-PCR analysis for OL-enriched THAP1-CNS genes on day 6 of T3 (−PDGF + T3)-mediated differentiation. RNA expression is normalized Olig2 expression and represented as fold change compared with day-0 OPC values . Graph shows mean values ± SEM. Significance values determined using t test (*$p < 0.05$ and ***$p < 0.001$; n.s., not significant).

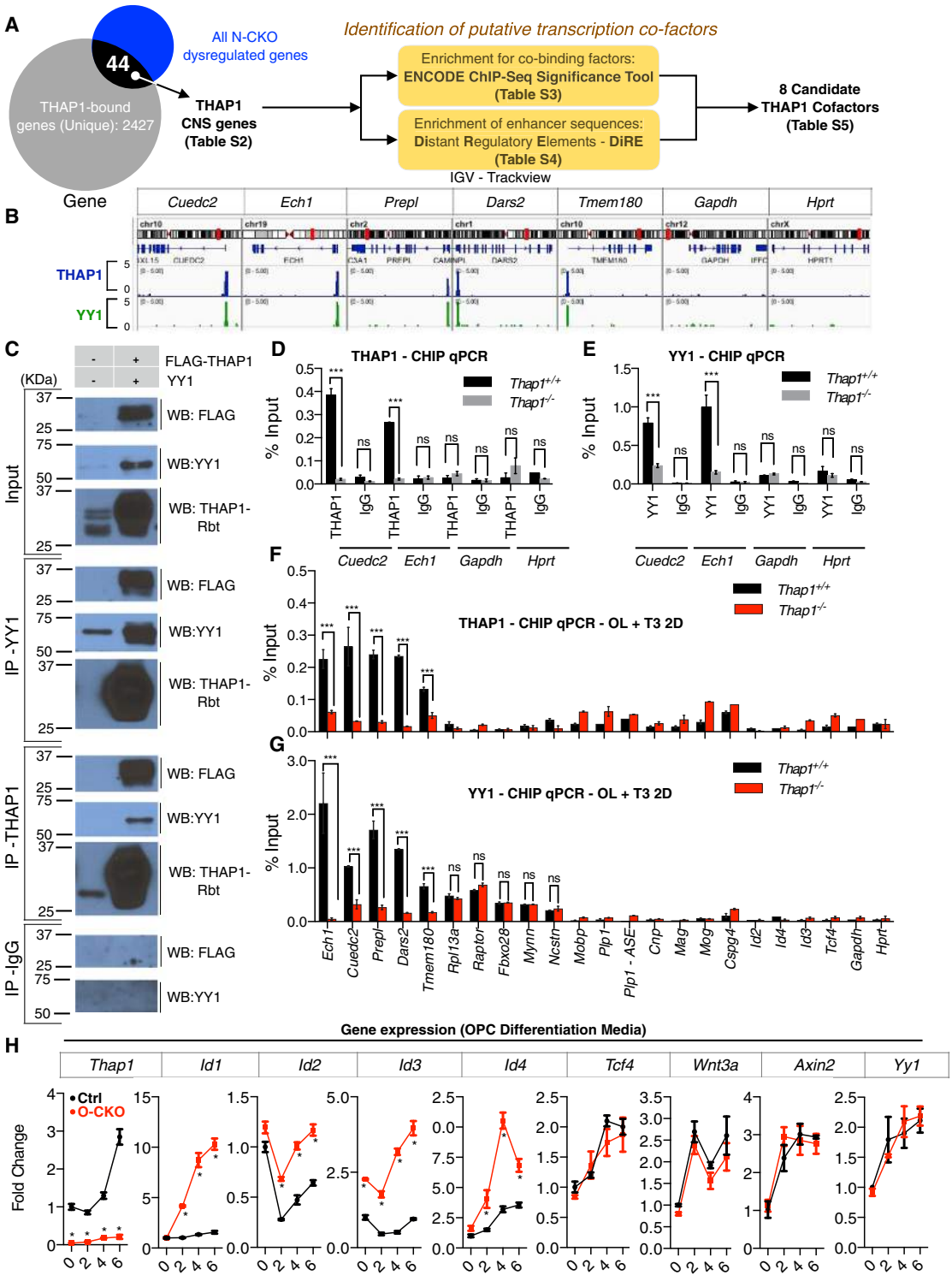

Figure 6. THAP1 Colocalizes with and Affects YY1 Occupancy

(A) Schematic of the strategy used to identify putative cofactors for THAP1. The genomic regions corresponding to TSS (±1 kb) of the 44 THAP1-CNS genes (genes bound and regulated by THAP1) were subjected to independent analyses to identify transcription factors with significantly enriched binding (ENCODE ChIP-seq Significance Tool) and significantly enriched DNA binding motifs (distant regulatory elements [DiRE]). Eight genes were identified in common in these analyses, which we define as putative THAP1-cofactors.

(B and D–G) THAP1 regulates YY1 occupancy in OL. (B) Genome Browser track (IGV) showing ChIP-seq signals for THAP1 and YY1 for five candidate genes (*Ech1*, *Cuedc2*,*Prepl*, *Dars2*, and *Tmem180*) and two control genes (*Gapdh* and *Hprt*). (D and E) Quantitative ChIP (qChIP) demonstrating specificity for antibodies

(legend continued on next page)

mutation. There is not a clear genotype-phenotype relationship between *THAP1* mutations and clinical phenotype (Xiromerisiou et al., 2012), indicating the existence of additional factors that determine disease severity.

Conditional CNS deletion of *Thap1* caused a striking defect in myelination that persisted during the first month of life. This defect was present broadly throughout the CNS and involved several myelin protein components, as demonstrated in western blot analyses of whole brain protein (Figures 1F and 1G) and ultrastructural studies of axons in ON and genu of CC (Figure 4). Such overt effects appeared limited to OL; we observed no evidence of axon damage at the morphological, protein or genetic levels (Figures S2C, S3C, 3A, and 3B). We cannot, however, exclude functional axonal defects with these analyses. Nevertheless, conditional deletion of *Thap1* from the OL lineage *in vivo* and in studies examining NSC developing into OL *in vitro* recapitulated the effects of *Thap1* deficiency on myelination. Considered together, these studies establish a cell-autonomous role for *Thap1* in the OL lineage that appears to be independent of axon-derived signals.

Notably, myelination deficits in *Thap1* null mice are severe during an early postnatal window. Abnormalities of myelin proteins and white matter-related structural defects are present from as early as P7, but assays measuring "bulk" myelin components (Figures 1F, 1G, 2G, 3A, and 3B) indicate that they resolve by ~8 weeks of age. mRNA analysis of CNS tissue from juvenile and adult animals continues to show complete absence of *Thap1* mRNA (Figure S1E), arguing against the possibility that the "catch-up" of myelination occurs from cells that escape genetic ablation. Indeed, ultrastructural data indicate that this "catch-up" may not be complete. EM analyses of the genu of CC in adult O-CKO mice demonstrate persistent hypomyelination, albeit of smaller effect size than in juvenile animals (Figures 4A–4E). These findings indicate that within the OL lineage *Thap1* function is particularly important during the early postnatal period.

A vulnerable period during early CNS maturation is consistent with the childhood onset of most subjects with DYT6 dystonia (Ozelius and Bressman, 2011). Neurodevelopmental vulnerable periods are also observed in mouse models of DYT1 dystonia (Liang et al., 2014; Pappas et al., 2015; Tanabe et al., 2016; Weisheit and Dauer, 2015), indicating a potential pathophysiological theme for childhood-onset dystonias. In contrast to the myelination defects, motor abnormalities persist in N-CKO mice. These data raise the possibility that, as in other neurodevelopmental diseases such as autism and schizophrenia (Connors et al., 2008; Hoftman and Lewis, 2011; Shaw et al., 2010), disrupting the highly dynamic developmental trajectory may cause abnormal circuit formation and persistent behavioral symptoms—even if the original insult (in this case, hypomyelination) resolves.

Mechanistically, THAP1 deficiency selectively disrupts later stages of OL lineage progression. Gene expression studies from *Thap1* null juvenile CNS and stereological analysis demonstrate normal numbers of OPC and no abnormality in the generation of immature OL (Figures 2D and 2E). A clear defect was observed in the progression to mature myelinating OL, however. These observations were recapitulated in *in vitro* studies of differentiating OL generated from purified OPC, emphasizing the cell-autonomous effects of THAP1 in this lineage. Previous work indicates a role for THAP1 in cell-cycle pathways, suggesting that it regulates cell-cycle and apoptotic genes (in HUVECs; Cayrol et al., 2007). While germline deletion of *Thap1* causes embryonic lethality, we did not observe growth defects in *Thap1* null mouse stem cells, NSC, or OPC (data not shown), and gene expression studies indicate that *Thap1* null OPC exit the cell cycle normally (Figure 5F). Furthermore, conditional CNS deletion of *Thap1* did not appear to disrupt the generation of neurons, as the brains of N-CKO mice appear grossly normal by routine histological studies (data not shown). Considered together, these observations and those in another model of DYT6 dystonia (Ruiz et al., 2015) indicate that dysregulation of cell-cycle pathways is unlikely to be responsible for THAP1 LOF abnormalities within the CNS, the tissue most relevant to DYT6 dystonia.

How might THAP1 deficiency disrupt OL maturation? Our findings suggest that THAP1 functions with YY1, a transcription factor with a well-established role in OL maturation. Analysis of genomic regions neighboring the TSS of THAP1-bound genes demonstrates that >95% of THAP1-associated genes were also bound (and at similar regions) by YY1. These findings are consistent with recent work reporting co-enrichment of YY1 and THAP1 DNA binding motifs (Kheradpour and Kellis, 2014; Aguilo et al., 2017). Loss of THAP1 significantly decreased the occupancy of YY1 at all five candidate target genes tested in both ESC and OL cells, mimicking YY1 LOF at these loci. Prior studies have established YY1 as essential for OL maturation and demonstrated that conditional loss of YY1 in OL lineage disrupts CNS myelination (He et al., 2007). Interestingly, both THAP1 and YY1 associate with the TSS of the *Thap1* gene both in the ChIP-seq database and our ChIP studies in ESC (Figure S5C), raising the possibility that YY1 may regulate *Thap1*.

(goat anti-THAP1 and rabbit anti-YY1) used in ChIP studies. Binding, represented as percent input (y axis) demonstrated for (D) THAP1 and (E) YY1 and their respective isotype control IgG (goat IgG or rabbit IgG) for candidate genes (*Ech1*, *Cuedc2*, *Gapdh*, and *Hprt*) tested (x axis). The y axis (percent input) represents the final amount of immunoprecipitated chromatin/gene assessed as the percentage of total input chromatin from corresponding control ($Thap1^{+/+}$) and *Thap1* null ESC ($Thap1^{-/-}$) (STAR Methods). Graph shows mean values ± SEM. (F and G) qChIP demonstrating binding represented as percent input (y axis) for THAP1 (E) and YY1 (F) in control *Thap1* null OL cells at the 22 gene loci tested (x axis). Graph shows mean values ± SEM.

(C) Coimmunoprecipitation demonstrating THAP1 interactions with YY1. HEK293T cells transfected with YY1 and THAP1-FLAG1 was immunoprecipitated with goat anti-THAP1, rabbit anti-YY1, or normalized rabbit IgG and immunoblotted with anti-FLAG, YY1, or rabbit anti-THAP1.

(H) Id genes are selectively upregulated in *Thap1* null OL. qRT-PCR is depicted for multiple days (x axis) following PDGF withdrawal for candidate genes regulated by BMP pathway. Gene expression values are normalized to *Olig2* expression and represented as fold change (y axis) compared with day-0 OPC values. Two-way ANOVA demonstrates a main effect of genotype ($p < 0.01$) for all genes shown in (G). Asterisks represent time points where significant differences exist using Sidak's post hoc multiple comparison test. Note that the expression of *Thap1* in (H) is reproduced (Figure 5I) for clarity of comparisons in differentiation gene expression. Graph shows mean values ± SEM.

Significance values in (D) and (E) were determined using t test: ***$p < 0.001$; n.s., not significant.

These observations establish a fundamental functional relationship of THAP1 and YY1 and suggest that these proteins may be coregulators of genes essential for OL lineage progression.

The mechanism whereby YY1 deficiency impairs OL maturation deficits is not completely understood. Little evidence suggests that YY1 associates directly with genes encoding myelin components. We explored a direct role for YY1 (and THAP1) at myelin genes in OL cells, finding that neither exhibits significant association at any of the six myelination genes tested (Figures 6F and 6G). In contrast, we find that Id genes are robustly upregulated in *Thap1* null OL cells, as observed following YY1 loss (He et al., 2007). Consistent with these findings, a recent THAP1 CHIP-seq study conducted in mouse embryonic stem cells shows no evidence of THAP1 association with core myelin component or Id genes (Aguilo et al., 2017). ID2 and ID4 are members of the inhibitor of differentiation (ID) family of helix-loop-helix transcriptional inhibitors that play an essential role in the maintenance of OPC state and the timing of differentiation into mature OL cells (Jessen and Mirsky, 2008; Kondo and Raff, 2000; Samanta and Kessler, 2004). The upregulation of these ''maturation-inhibitory'' genes in differentiating *Thap*1 null OL is consistent with our observation both *in vivo* and *in vitro* that THAP1 loss does not affect the status of OPC. While the mechanism whereby loss of THAP1 and YY1 upregulate *Id* genes remains to be determined, this shared phenotype mechanistically links these genes to a core molecular mechanism controlling OL lineage differentiation.

Our findings establish a biological role for THAP1 in the CNS and demonstrate a direct molecular link between myelination pathways and childhood-onset dystonia. The cell-autonomous role of THAP1 in oligodendrocytes and the neurodevelopmental specificity of THAP1 effects *in vivo* will provide focal points for future studies of dystonia and may enable fundamental insights into the mechanisms of progression through the OL lineage. These findings also raise the possibility that future screening of additional patient populations may extend the disease-relevant spectrum of THAP1 dysfunction to neurodevelopmental leukodystrophies.

STAR★METHODS

Detailed methods are provided in the online version of this paper and include the following:

- KEY RESOURCES TABLE
- CONTACT FOR REAGENT AND RESOURCE SHARING
- EXPERIMENTAL MODEL AND SUBJECT DETAILS
- METHOD DETAILS
  - Generation and Maintenance of Mice
  - Protein Extraction, Immunoprecipitation, and Western Blotting
  - RNA Extraction, qRT-PCR and Microarray
  - Histology and Immunohistochemistry
  - Cell Counting, CC Volume and Cortical Thickness Estimation
  - Motor Behavior Tests
  - Electron Microscopy
  - Derivation of OPC from NSC Cells
  - Quantitative Chromatin Immunoprecipitation (qChIP)
- QUANTIFICATION AND STATISTICAL ANALYSIS
- DATA AND SOFTWARE AVAILABILITY

SUPPLEMENTAL INFORMATION

Supplemental Information includes five figures, six tables, and one movie and can be found with this article online at http://dx.doi.org/10.1016/j.devcel.2017.06.009.

AUTHOR CONTRIBUTIONS

D.Y. and W.T.D. designed research; R.K., M.R.C., C.-C.L., and D.Y. performed and analyzed microarray data; A.Y., R.M., and D.Y. performed western blots, gene expression analyses, and EM studies; S.J. performed all behavioral analyses; S.S.P. and S.P. performed and analyzed stereology; S.P. and D.Y. performed all *in vitro* experiments; D.Y. performed ChIP experiments; D.Y., C.-C.L., and S.S.P. performed statistical analysis; D.Y. and W.D. wrote the manuscript with input from all authors.

ACKNOWLEDGMENTS

We are grateful to Dr. Roman Giger and Dr. Yevgeniya Mironova for providing us with many reagents and valuable discussions. We thank Alexander Hodge and Audrey Kim for technical assistance. We thank the laboratory of Dr. Stanley Watson for providing access to their microscope and support for the use of stereoinvestigator software. We thank Drs. Catherine Collins, Paul Jenkins, Roman Giger, and Tony Antonellis for critical reading of the manuscript. We thank the Jeff Harrison and Pennelope Blakely (MIL, University of Michigan), Hong Yi (EM Core, Emory University), and the rest of the staff of University of Michigan's Core Facilities (DNA Sequencing Core, Unit of Laboratory Animal Medicine) and the Gene Targeting and Transgenic Facility at UCONN Health. This research was supported in part by the following grants: RO1NS077730 to W.T.D. (NINDS), Dystonia Medical Research Foundation to W.T.D., UM Center for Organogenesis Training Program and NCATS (NIH, Award Number 2UL1TR000433) to D.Y., and Intramural Research Program of the NIH, National Institute on Aging to M.R.C.

Received: August 26, 2016
Revised: April 25, 2017
Accepted: June 7, 2017
Published: July 10, 2017

REFERENCES

Aguilo, F., Zakirova, Z., Nolan, K., Wagner, R., Sharma, R., Hogan, M., Wei, C., Sun, Y., Walsh, M.J., Kelley, K., Zhang, W., et al. (2017). THAP1: role in mouse embryonic stem cell survival and differentiation. Stem Cell Rep. http://dx.doi.org/10.1016/j.stemcr.2017.04.032.

Auerbach, R.K., Chen, B., and Butte, A.J. (2013). Relating genes to function: identifying enriched transcription factors using the ENCODE ChIP-Seq significance tool. Bioinformatics *29*, 1922–1924.

Berndt, J.A., Kim, J.G., Tosic, M., Kim, C., and Hudson, L.D. (2001). The transcriptional regulator Yin Yang 1 activates the myelin PLP gene. J. Neurochem. *77*, 935–942.

Blanchard, A., Ea, V., Roubertie, A., Martin, M., Coquart, C., Claustres, M., Beroud, C., and Collod-Beroud, G. (2011). DYT6 dystonia: review of the literature and creation of the UMD Locus-Specific Database (LSDB) for mutations in the THAP1 gene. Hum. Mutat. *32*, 1213–1224.

Bonilha, L., de Vries, P.M., Vincent, D.J., Rorden, C., Morgan, P.S., Hurd, M.W., Besenski, N., Bergmann, K.J., and Hinson, V.K. (2007). Structural white matter abnormalities in patients with idiopathic dystonia. Mov. Disord. *22*, 1110–1116.

Campagne, S., Saurel, O., Gervais, V., and Milon, A. (2010). Structural determinants of specific DNA-recognition by the THAP zinc finger. Nucleic Acids Res. *38*, 3466–3476.

Carbon, M., Argyelan, M., Ghilardi, M.F., Mattis, P., Dhawan, V., Bressman, S., and Eidelberg, D. (2011). Impaired sequence learning in dystonia mutation carriers: a genotypic effect. Brain *134*, 1416–1427.

Cayrol, C., Lacroix, C., Mathe, C., Ecochard, V., Ceribelli, M., Loreau, E., Lazar, V., Dessen, P., Mantovani, R., Aguilar, L., et al. (2007). The THAP-zinc finger protein THAP1 regulates endothelial cell proliferation through modulation of pRB/E2F cell-cycle target genes. Blood *109*, 584–594.

Cheng, F.B., Wan, X.H., Feng, J.C., Ma, L.Y., Hou, B., Feng, F., Wang, L., and Yang, Y.M. (2012). Subcellular distribution of THAP1 and alterations in the microstructure of brain white matter in DYT6 dystonia. Parkinsonism Relat. Disord. *18*, 978–982.

Connors, S.L., Levitt, P., Matthews, S.G., Slotkin, T.A., Johnston, M.V., Kinney, H.C., Johnson, W.G., Dailey, R.M., and Zimmerman, A.W. (2008). Fetal mechanisms in neurodevelopmental disorders. Pediatr. Neurol. *38*, 163–176.

Dauer, W. (2014). Inherited isolated dystonia: clinical genetics and gene function. Neurotherapeutics *11*, 807–816.

Dean, D.C., 3rd, O'Muircheartaigh, J., Dirks, H., Waskiewicz, N., Walker, L., Doernberg, E., Piryatinsky, I., and Deoni, S.C. (2015). Characterizing longitudinal white matter development during early childhood. Brain Struct. Funct. *220*, 1921–1933.

Dugas, J.C., and Emery, B. (2013). Purification of oligodendrocyte precursor cells from rat cortices by immunopanning. Cold Spring Harb. Protoc. *2013*, 745–758.

Fuchs, T., Gavarini, S., Saunders-Pullman, R., Raymond, D., Ehrlich, M.E., Bressman, S.B., and Ozelius, L.J. (2009). Mutations in the THAP1 gene are responsible for DYT6 primary torsion dystonia. Nat. Genet. *41*, 286–288.

Gabriele, M., Vulto-van Silfhout, A.T., Germain, P.L., Vitriolo, A., Kumar, R., Douglas, E., Haan, E., Kosaki, K., Takenouchi, T., Rauch, A., et al. (2017). YY1 Haploinsufficiency causes an intellectual disability syndrome featuring transcriptional and chromatin dysfunction. Am. J. Hum. Genet. *100*, 907–925.

Gotea, V., and Ovcharenko, I. (2008). DiRE: identifying distant regulatory elements of co-expressed genes. Nucleic Acids Res. *36*, W133–W139.

Guo, W., Patzlaff, N.E., Jobe, E.M., and Zhao, X. (2012). Isolation of multipotent neural stem or progenitor cells from both the dentate gyrus and subventricular zone of a single adult mouse. Nat. Protoc. *7*, 2005–2012.

He, Y., Dupree, J., Wang, J., Sandoval, J., Li, J., Liu, H., Shi, Y., Nave, K.A., and Casaccia-Bonnefil, P. (2007). The transcription factor Yin Yang 1 is essential for oligodendrocyte progenitor differentiation. Neuron *55*, 217–230.

Heng, M.Y., Lin, S.T., Verret, L., Huang, Y., Kamiya, S., Padiath, Q.S., Tong, Y., Palop, J.J., Huang, E.J., Ptacek, L.J., et al. (2013). Lamin B1 mediates cell-autonomous neuropathology in a leukodystrophy mouse model. J. Clin. Invest. *123*, 2719–2729.

Hoftman, G.D., and Lewis, D.A. (2011). Postnatal developmental trajectories of neural circuits in the primate prefrontal cortex: identifying sensitive periods for vulnerability to schizophrenia. Schizophr. Bull. *37*, 493–503.

Houlden, H., Schneider, S.A., Paudel, R., Melchers, A., Schwingenschuh, P., Edwards, M., Hardy, J., and Bhatia, K.P. (2010). THAP1 mutations (DYT6) are an additional cause of early-onset dystonia. Neurology *74*, 846–850.

Jessen, K.R., and Mirsky, R. (2008). Negative regulation of myelination: relevance for development, injury, and demyelinating disease. Glia *56*, 1552–1565.

Kheradpour, P., and Kellis, M. (2014). Systematic discovery and characterization of regulatory motifs in ENCODE TF binding experiments. Nucleic Acids Res. *42*, 2976–2987.

Kondo, T., and Raff, M. (2000). The Id4 HLH protein and the timing of oligodendrocyte differentiation. EMBO J. *19*, 1998–2007.

Liang, C.C., Tanabe, L.M., Jou, S., Chi, F., and Dauer, W.T. (2014). TorsinA hypofunction causes abnormal twisting movements and sensorimotor circuit neurodegeneration. J. Clin. Invest. *124*, 3080–3092.

Mazars, R., Gonzalez-de-Peredo, A., Cayrol, C., Lavigne, A.C., Vogel, J.L., Ortega, N., Lacroix, C., Gautier, V., Huet, G., Ray, A., et al. (2010). The THAP-zinc finger protein THAP1 associates with coactivator HCF-1 and O-GlcNAc transferase: a link between DYT6 and DYT3 dystonias. J. Biol. Chem. *285*, 13364–13371.

Ortiz-Virumbrales, M., Ruiz, M., Hone, E., Dolios, G., Wang, R., Morant, A., Kottwitz, J., Ozelius, L.J., Gandy, S., and Ehrlich, M.E. (2014). Dystonia type 6 gene product Thap1: identification of a 50 kDa DNA-binding species in neuronal nuclear fractions. Acta Neuropathol. Commun. *2*, 139.

Ozelius, L.J., and Bressman, S.B. (2011). Genetic and clinical features of primary torsion dystonia. Neurobiol. Dis. *42*, 127–135.

Pappas, S.S., Leventhal, D.K., Albin, R.L., and Dauer, W.T. (2014). Mouse models of neurodevelopmental disease of the basal ganglia and associated circuits. Curr. Top. Dev. Biol. *109*, 97–169.

Pappas, S.S., Darr, K., Holley, S.M., Cepeda, C., Mabrouk, O.S., Wong, J.M., LeWitt, T.M., Paudel, R., Houlden, H., Kennedy, R.T., et al. (2015). Forebrain deletion of the dystonia protein torsinA causes dystonic-like movements and loss of striatal cholinergic neurons. Elife *4*, e08352.

Ramdhani, R.A., and Simonyan, K. (2013). Primary dystonia: conceptualizing the disorder through a structural brain imaging lens. Tremor Other Hyperkinet. Mov. (N Y) *3*, http://dx.doi.org/10.7916/D8H70DJ7.

Roussigne, M., Cayrol, C., Clouaire, T., Amalric, F., and Girard, J.P. (2003). THAP1 is a nuclear proapoptotic factor that links prostate-apoptosis-response-4 (Par-4) to PML nuclear bodies. Oncogene *22*, 2432–2442.

Ruiz, M., Perez-Garcia, G., Ortiz-Virumbrales, M., Meneret, A., Morant, A., Kottwitz, J., Fuchs, T., Bonet, J., Gonzalez-Alegre, P., Hof, P.R., et al. (2015). Abnormalities of motor function, transcription and cerebellar structure in mouse models of THAP1 dystonia. Hum. Mol. Genet. *24*, 7159–7170.

Sabogal, A., Lyubimov, A.Y., Corn, J.E., Berger, J.M., and Rio, D.C. (2010). THAP proteins target specific DNA sites through bipartite recognition of adjacent major and minor grooves. Nat. Struct. Mol. Biol. *17*, 117–123.

Salmaso, N., Jablonska, B., Scafidi, J., Vaccarino, F.M., and Gallo, V. (2014). Neurobiology of premature brain injury. Nat. Neurosci. *17*, 341–346.

Samanta, J., and Kessler, J.A. (2004). Interactions between ID and OLIG proteins mediate the inhibitory effects of BMP4 on oligodendroglial differentiation. Development *131*, 4131–4142.

Schneider, S.A., Ramirez, A., Shafiee, K., Kaiser, F.J., Erogullari, A., Bruggemann, N., Winkler, S., Bahman, I., Osmanovic, A., Shafa, M.A., et al. (2011). Homozygous THAP1 mutations as cause of early-onset generalized dystonia. Mov. Disord. *26*, 858–861.

Sengel, C., Gavarini, S., Sharma, N., Ozelius, L.J., and Bragg, D.C. (2011). Dimerization of the DYT6 dystonia protein, THAP1, requires residues within the coiled-coil domain. J. Neurochem. *118*, 1087–1100.

Shaw, P., Gogtay, N., and Rapoport, J. (2010). Childhood psychiatric disorders as anomalies in neurodevelopmental trajectories. Hum. Brain Mapp. *31*, 917–925.

Soriano, P. (1999). Generalized lacZ expression with the ROSA26 Cre reporter strain. Nat. Genet. *21*, 70–71.

Standaert, D.G. (2011). Update on the pathology of dystonia. Neurobiol. Dis. *42*, 148–151.

Tanabe, L.M., Kim, C.E., Alagem, N., and Dauer, W.T. (2009). Primary dystonia: molecules and mechanisms. Nat. Rev. Neurol. *5*, 598–609.

Tanabe, L.M., Liang, C.C., and Dauer, W.T. (2016). Neuronal nuclear membrane budding occurs during a developmental window modulated by torsin paralogs. Cell Rep. *16*, 3322–3333.

van der Meer, J.N., Beukers, R.J., van der Salm, S.M., Caan, M.W., Tijssen, M.A., and Nederveen, A.J. (2012). White matter abnormalities in gene-positive myoclonus-dystonia. Mov Disord. *27*, 1666–1672.

Weisheit, C.E., and Dauer, W.T. (2015). A novel conditional knock-in approach defines molecular and circuit effects of the DYT1 dystonia mutation. Hum. Mol. Genet. *24*, 6459–6472.

Winters, J.J., Ferguson, C.J., Lenk, G.M., Giger-Mateeva, V.I., Shrager, P., Meisler, M.H., and Giger, R.J. (2011). Congenital CNS hypomyelination in the Fig4 null mouse is rescued by neuronal expression of the PI(3,5)P(2) phosphatase Fig4. J. Neurosci. *31*, 17736–17751.

Xiao, L., Ohayon, D., McKenzie, I.A., Sinclair-Wilson, A., Wright, J.L., Fudge, A.D., Emery, B., Li, H., and Richardson, W.D. (2016). Rapid production of new oligodendrocytes is required in the earliest stages of motor-skill learning. Nat. Neurosci. *19*, 1210–1217.

Xiromerisiou, G., Houlden, H., Scarmeas, N., Stamelou, M., Kara, E., Hardy, J., Lees, A.J., Korlipara, P., Limousin, P., Paudel, R., et al. (2012). THAP1 mutations and dystonia phenotypes: genotype phenotype correlations. Mov. Disord. *27*, 1290–1294.

Yellajoshyula, D., Patterson, E.S., Elitt, M.S., and Kroll, K.L. (2011). Geminin promotes neural fate acquisition of embryonic stem cells by maintaining chromatin in an accessible and hyperacetylated state. Proc. Natl. Acad. Sci. USA *108*, 3294–3299.

Zhang, Y., Chen, K., Sloan, S.A., Bennett, M.L., Scholze, A.R., O'Keeffe, S., Phatnani, H.P., Guarnieri, P., Caneda, C., Ruderisch, N., et al. (2014). An RNA-sequencing transcriptome and splicing database of glia, neurons, and vascular cells of the cerebral cortex. J. Neurosci. *34*, 11929–11947.

Zolova, O.E., and Wight, P.A. (2011). YY1 negatively regulates mouse myelin proteolipid protein (Plp1) gene expression in oligodendroglial cells. ASN Neuro *3*, http://dx.doi.org/10.1042/AN20110021.

STAR★METHODS

KEY RESOURCES TABLE

REAGENT or RESOURCE	SOURCE	IDENTIFIER
Antibodies		
Goat anti-THAP1	Santacruz	Cat# sc-98174; RRID: AB_2201675
Rabbit anti-THAP1	Proteintech	Cat# 12584-1-AP; RRID: AB_2201672
Rabbit anti-YY1	Santacruz	Cat# sc-281; RRID: AB_2218504
Mouse anti-YY1	Santacruz	Cat# sc-7341; RRID: AB_2257497
Normalized anti-Rabbit IgG	Santacruz	Cat# sc-2027; RRID: AB_737197
Rat anti-MBP	Millipore	Cat# MAB386; RRID: AB_94975
Mouse anti-Actin	Sigma	Cat# 5316; RRID: AB_476743
Rabbit anti-MOBP	One World Lab	Cat# AP6913a; RRID: AB_1967959
Mouse anti-MOG	Millipore	Cat# MAB5680; RRID: AB_1587278
Mouse anti-CNP	Sigma	Cat# C5922; RRID: AB_476854
Mouse anti-β III - TUBULIN	Millipore	Cat# MAB1637; RRID: AB_2210524
Rabbit anti-PLP1	This Study	Provided by Dr. Roman Giger, University of Michigan
Rabbit anti-MAG	This Study	Provided by Dr. Roman Giger, University of Michigan
Mouse anti-MAG	Millipore	Cat# MAB1567; RRID: AB_2137847
HRP conjugated Donkey Anti-Rabbit	Thermofisher Sceintific	Cat# 31402; RRID: AB_228395
HRP conjugated Donkey Anti-Mouse	Jackson Immunoresearch	Cat# 115-035-003; RRID: AB_10015289
Chemicals, Peptides, and Recombinant Proteins		
Murine FGF2	Peprotech	Cat# 450-33
Murine EGF	Peprotech	Cat# AF-100-15
Murine PDGF-AA	Peprotech	Cat# 315-17
RAT CNTF	Peprotech	Cat# 450-50
Human NT3	Peprotech	Cat# 450-03
2x SYBR Green qPCR Master Mix	Bimake	Cat# B21202
Dynabeads ProteinG	Thermofisher	Cat# 10003D
Purmorphamine	Cayman Chemical	Cat# 483367-10-8
Neurobasal	Thermofisher	Cat# 21103049
DMEM/F12	Thermofisher	Cat# 11320-033
DMEM High Glucose	Thermofisher	Cat# 11995040
Critical Commercial Assays		
VECTASTAIN ELITE ABC Kit	Vector Laboratories	Cat# PK-6100; RRID: AB_2336819
SMART MMLV Reverse Transcriptase	Clontech	Cat# 639522
Quick-RNA MicroPrep	Zymo Research	Cat# R1050
Deposited Data		
Microarray	This Study	GEO: GSE97372
Chip-Seq THAP1	ENCODE	GEO: GSM803408
Chip-Seq YY1	ENCODE	GEO: GSM803446
Experimental Models: Cell Lines		
Neural Stem Cells - NSC	This Study	N/A
Oligodendrocyte Progenitor Cells - OPC	This Study	N/A
HEK-293	ATCC	CRL-1573
Oligonucleotides		
lox-F	This Study	TGCTGGGTGTTGGAAAATAA
frt-F	This Study	GCATAGGACAGAGCCTTTCAG

(*Continued on next page*)

Continued

REAGENT or RESOURCE	SOURCE	IDENTIFIER
frt-R	This Study	GATGCCAATACCTGATTGGAG
qRT - PCR	This Study	Table S6
qChIP - PCR	This Study	Table S6
Recombinant DNA		
pSPORT-YY1	GE Dharmacon	MMM1013-202761238
pDEST26 – FLAG-THAP1	This Study	N/A
pDEST26 – THAP1	This Study	N/A
Software and Algorithms		
Image J	NIH	https://imagej.nih.gov/ij/
Graphed Prism	GraphPad	https://graphpad.com/scientific-software/prism/

CONTACT FOR REAGENT AND RESOURCE SHARING

Further information and requests for reagents should be directed to and will be fulfilled by the Lead Contact, William T. Dauer (dauer@med.umich.edu).

EXPERIMENTAL MODEL AND SUBJECT DETAILS

Animal testing was conducted in accord with the NIH laboratory animal care guidelines and with the Institutional Animal Care and Use Committee (IACUC) at the University of Michigan.

METHOD DETAILS

Generation and Maintenance of Mice

Thap1 floxed mice were generated in collaboration with the Gene Targeting and Transgenic Facility at UCONN Health. Chimeras with *Thap1* flox allele were bred to ROSA26-FLPe mice to remove the frt-flanked neomycin resistance gene, generating the floxed allele used for all studies (Liang et al., 2014). To genotype these *Thap1* mutants, we used the primers: lox-F, frt-F, & frt-R (Key Resources Table). These primers produce the following band sizes on PCR: WT, 273 bp; KO, 470 bp; floxed allele, 351 bp. The breeding strategy used to generate conditional null animals was as follows: $Thap1^{+/-}$, Cre^{+} × $Thap1^{flox/flox}$. This breeding strategy produced the following offspring: $Thap1^{flox/+}$; $Thap1^{flox/-}$; $Thap1^{flox/+}$, Cre^{+}; and $Thap1^{flx/-}$, Cre^{+} (CKO). Nestin-*Cre*+ and Hprt-*Cre*) mice were purchased from Jackson Laboratory (Bar Harbor, ME, USA). Olig2-*Cre* mice were kindly provided by Dr. Roman Giger. Age and sex-matched littermate mice were used for all experiments.

Protein Extraction, Immunoprecipitation, and Western Blotting

Total forebrain homogenates from mouse brain tissues were prepared using lysis buffer (50mM Tris pH8.0, 150 mM NaCl, 1% Triton X-100, 1mM EDTA, 1mM EGTA, 0.2% SDS and 1% NP40) supplemented with protease inhibitors (Roche), and were probed with the following antibodies: Anti-PLP1 and MAG (kindly provided by.Dr. Roman Giger), MBP (MAB386, Millipore), ACTIN (A5316, Sigma), CNP (C5922, Sigma), MOBP (AP6913a, One World Lab), MOG (MAB5680, Millipore) an TuJ1 (MAB1637, Millipore). Secondary HRP conjugated Donkey Anti-Rabbit (31402, Pierce) and Mouse (115-035-003, Jackson Immunoresearch) antibodies were used.

Coimmunoprecipitation experiment was conducted as previously described with minor modifications (Mazars et al., 2010). Briefly, nuclear extract was prepared in IP buffer (20mM Tris,pH7,4; 400mM NaCl, 5 mM MgCl2 , 10 mM β-mercaptoethanol, 0,5% Nonidet, 1 mM PMSF, and Complete protease inhibitor mixture,Bimake) and incubated overnight with anti-THAP1 (sc-98174, Santacruz), anti-YY1 (sc-281, Santacruz) or normalized anti-Rabbit IgG (sc-2027) that was pre-bound to Dynabeads (Thermofisher) as per manufacturers instructions. Followed by the precipitation of the proteins, the antibody-bead complex was washed extensively in IP buffer, eluted in 1x running buffer for 15 minutes at room temperature and analyzed using western blot.

RNA Extraction, qRT-PCR and Microarray

Total RNA was extracted with Trizol (Invitrogen) and used for cDNA synthesis with MMLV Reverse Transcriptase (Clontech) as per manufacturers instructions. Quantitative real time PCR (qRT–PCR) was performed with the 7500 HT real-time PCR Detection System (ABI) and 2x SYBR Green qPCR Master Mix (High ROX) (Bimake). Primer sequences for qPCR are provided in Table S6. Microarray analysis was performed on Illumina BeadChip Array MouseRef-8 v2 chips (BD-202-0202,Illumina) from total RNA extracted from P21 cortex or striatum (N=4). Analysis was performed using Beadstudio 3.1 software.

Histology and Immunohistochemistry

Brains were collected and sectioned for free floating immunohistochemistry (IHC). Consecutive 40 μm (for cell counting) or 60 μm (for CC volume measurement) coronal sections were generated on a cryostat and stained as previously described (Pappas et al., 2015). Primary Anti-MBP (MAB386, Millipore), MAG (MAB1567, Millipore), PDGFRα (14-1401-81, Affymetrix), NG2 (AB5320, Millipore), TuJ1 (MAB1637, Millipore) and APC/CC1 (OP80, Millipore) and secondary biotin conjugated Donkey Anti-Rabbit (711-065-152, Jackson Immunoresearch) and Mouse (115-065-003, Jackson Immunoresearch) were used for IHC. .

Cell Counting, CC Volume and Cortical Thickness Estimation

The number of OL in the motor cortex and corpus callosum (CC) were quantified using unbiased stereology. Stained serial sections were observed on a Zeiss Axioimager M2 and the motor cortex and CC were outlined using Stereoinvestigator software (MBF Bioscience, Williston, VT). Every sixth section was analyzed with the optical fractionator probe and 63x objective lens, with the following parameters.

Cell Marker (Antibody)	Counting Frame (μm)	Grid Size (μm)
PDGFRα	80X70	250X250
APC (CC1)	80X70	250X250
MAG	90X70	200X200
MBP	90X70	200X200

CC Volume was estimated using the Cavalieri probe in Stereoinvestigator (MBF Bioscience, Williston, VT). Ten unilateral coronal MBP or MAG stained serial sections (60 μm, every 6th section) were observed per brain and points within the CC were marked using a 60 μm grid. The final volumes were averaged from 5 animals per group.

Cortical thickness was estimated as the average length from the dorsal boundary of the CC to the outer edge of cortical layer 1 in six serial coronal sections (5 brains per genotype) as previously described (Pappas et al., 2015).

Motor Behavior Tests

Beam-cross, tail-suspension and open field tests were conducted as previously described (Liang et al., 2014; Pappas et al., 2015).

Electron Microscopy

P21 mice were anesthetized with a mixture of ketamine and xylazine and perfused with EM perfusion solution (3 % Paraformaldehyde, 2.5% glutaraldehyde (Electron Microscopy Sciences) in 0.1 M Phosphate buffer). Following the perfusion, brain and optic nerve was dissected and postfixed at 4°C overnight in perfusion solution and optic nerve EM solution (3 % Paraformaldehyde, 2.5% glutaraldehyde in 0.1 M Sorensen's buffer) respectively. Optic nerve was processed and sectioned as previously described (Winters et al., 2011) with the help of University of Michigan, MIL core services. Genu of CC was dissected, processed and sectioned at EM core facility, Emory University. All EM images were acquired using JEOL JSM 1400 at the University of Michigan, MIL core services. G-ratio was calculated as the ratio of the inner axonal diameter to total (including myelin) outer diameter) as previously described (Winters et al., 2011).

Derivation of OPC from NSC Cells

NSC were isolated from the SVZ of P7 mouse pups and propagated in NSC growth media (Neurobasal media supplemented with 1x B27, 1x Antibiotic-Antimycotic, 1x Glutamax, 20 ng/μl Fgf2 (Peprotech) and 20 ng/μl Egf2 (Peprotech)) as neurospheres in low attachment dishes as previously described (Guo et al., 2012). NSC were further expanded and grown as a monolayer on laminin coated dishes in NSC expansion media (DMEM/F12 media supplemented with 1x N2, 1x AA, 1x Glutamax, 20 ng/μl Fgf2 and 20 ng/μl Egf2). 1 × 10^4 NSC cells/cm^2 were grown as neurospheres in low attachment dishes in OPC expansion media (SATO medium (Dugas and Emery, 2013) supplemented with 30 ng/μl PDGF-AA (Peprotech), 20 ngl/ul Fgf2 and and 0.5 μM Purmorphamine (Cayman) for 4 days. Further expansion and growth of the OPC was done as a monolayer on poly-ornithine and laminin coated dishes in OPC expansion media (without Fgf2) for 2 - 3 weeks followed by which aliquot of cells were stored in 1x freezing media (Gibco). These isolated OPC cells were either expanded in OPC expansion media or differentiated in oligodendrocyte differentiation medium (SATO media without PDGF or Fgf2) with or without T3, 3,3',5-Triiodo-L-thyronine (Cayman).

Quantitative Chromatin Immunoprecipitation (qChIP)

qChIP was performed as previously described (Yellajoshyula et al., 2011). Sheared chromatin (sonicated to 200–500 bp) from 1 × 10^6 mouse ES cells was incubated with 2.5 μg of Goat anti-THAP1 (sc-98174, Santacruz), Rabbit anti-YY1 (sc-281, Santacruz) or normalized Rabbit IgG using Dynabeads (Invitrogen). After washing, elution and cross-link reversal, DNA from each ChIP sample and the corresponding input sample was purified and analyzed further using qPCR. Each ChIP sample and a range of dilutions of the corresponding input sample (0.01 – 2% input) were quantitatively analyzed with gene-specific primers using the 7500 HT detection system (ABI) and SYBR qPCR Premix (Clontech).

QUANTIFICATION AND STATISTICAL ANALYSIS

All data are reported as mean ± SEM with the exception of qRT-PCR which is represented as mean ± SD. All statistical tests reported (Student's t-tests, Chi square tests, One-way or two-way ANOVAs) were performed using Graphpad Prism software (version 6).

Quantification of immunofluorescence images was done after converting them to 8-bit images using ImageJ software.

DATA AND SOFTWARE AVAILABILITY

The accession number for microarray data reported in this manuscript is GEO: GSE97372. The accession number for ChIP-seq data used in manuscript for THAP1 is GEO: GSM803408 and for YY1 is GEO: GSM803446.